Al-doped Zinc Oxide as a Transparent Conductive Material

A thesis

submitted in partial fulfilment

of the requirements for the Degree

of

Master of Science

at the

University of Waikato

by

R. A. Linklater

THE UNIVERSITY OF
WAIKATO
Te Whare Wānanga o Waikato

University of Waikato

2011

Abstract

ZnO powders containing from 1-8 atom% aluminium ions were prepared from aqueous citrate-aminoalcohol-based gels calcined at 500°C. The powders were characterized using ^{27}Al NMR, X-ray diffraction (XRD), and scanning electron microscopy (SEM). Solid state ^{27}Al NMR clearly distinguished between different Al environments and was effective in determining the relative amounts of incorporation of Al dopant ions into the different Zn lattice sites in the zincite structure. A degree of control over dopant placement is demonstrated by modifying sol precursors and processing parameters, which allowed a synthesis protocol to be developed to optimise the doping effectiveness. Relatively minor variations in processing conditions can influence the degree and mode of Al incorporation.

Thin films (*ca* 100 nm) were fabricated by spin-coating the Al-doped Zinc citrate sol-gels onto glass and quartz substrates, followed by a drying step and annealing at 500°C. The degree of crystal alignment in thin films, determined by X-ray diffraction studies, was found to be influenced by both the dopant level and the heating profile. Resistivity measurements showed films with 0.5-1atom %Al and multiple layers which had been heated at 90°C before annealing at 500°C, and subjected to post-annealing treatment under vacuum displayed the lowest resistivities. Further post-annealing treatment at 500°C under H_2/N_2 reduced resistivities by an order of magnitude.

Transparencies for all films were above 80% in the visible range, and thicker multi-layer films generally demonstrated lower transmittances. Preferential c-axis orientation was observed for all films, but showed higher intensities with increasing film thickness, and for films subjected to directional heating on a hotplate. Increased film thickness gave films with lower resistivities, but also lower transparencies

Acknowledgements

Thank you to my supervisors; Dr Tim Kemmitt for your day-to-day guidance and supervision of practical laboratory work, and to Professor Brian Nicholson for your patience and assistance throughout the writing process. I have learnt a lot from both of you.

I would also like to thank Dr Herbert Wong for his help with NMR spectroscopy and Martin Ryan for sharing his expertise in X-Ray diffraction techniques.

The research involving synchrotron experiments was undertaken on the powder diffraction beamline at the Australian Synchrotron, Victoria, Australia. I'd like to thank the beamline scientists, in particular Justin Kimpton, for all of their help. Also thanks to Dr. Bridget Ingham for facilitating this synchrotron research, and the processing and analyses of the resulting data, without whom I would have been lost.

I would like to thank Industrial Research Limited for the use of their resources, and the opportunity to participate in an area of research which would not otherwise have been open to me.

To my family and friends, no thanks would be enough for all of your patience and support.

Contents

List of Figures

List of Tables

Chapter 1

Introduction

This thesis reports investigations into producing Al-doped ZnO thin films from sol-gel precursors with optimised electrical and optical properties for use as transparent conductive materials. An ^{27}Al NMR study of the ZnO:Al bulk was carried out to determine the effect of processing parameters such as thermal treatment and dopant ion concentrations on the incorporation of Al into the zincite structure. The results from this study were then applied to thin films fabricated by spin coating of the same sol-gel precursors onto glass and quartz substrates. Resistivity and transparency measurements were made to determine the electrical and optical properties of the films, and conditions for producing optimised films were determined.

1.1 Zinc Oxide

ZnO is an n-type direct bandgap semiconductor. It possesses a wide bandgap, (3.3 eV), large free exciton binding energy, high carrier mobility with a wide range of resistivity (10^{-4}–10^{12} Ωcm), and high visible light transparency. Investigated as an electronic material since the 1930s, ZnO belongs to the class of transparent conducting oxides (TCOs). The other important oxides are in-

dium and tin oxide. Native ZnO is an interesting material due to its ease of handling, formation and tendency to form high aspect ratio crystallites.

One of the first practical applications of the semiconductor properties of zinc oxide was in the 1920s as detectors in build-your-own radio sets. The chemistry of ZnO is broad and varied, inciting the possibility of applications which make use of its inherent properties such as a low power threshold for optical pumping, radiation hardness and bio-compatibility. ZnO has performed better than GaN in terms of radiation resistance, making it a possible alternative for devices used in space and nuclear applications [1].

Studies on the properties of zinc oxide (ZnO) have been well reviewed [1–3] with a recent resurgence of research in this area due to the wide range of applications for which zinc oxide is suitable. Recently ZnO-based transparent thin films have generated significant interest for use in applications such as thin-film transistors, thin-film solar cells, transparent electronic circuits, and in flat panel displays [4–8].

ZnO films are commonly found in most thin film solar cells. There is a large focus on developing and improving the properties of these films so as to advance this technology as a suitable option for renewable energy. ZnO, as a high band gap semiconductor, shows properties such as larger bandgap and higher electron mobility, making it suitable for use in high power, high temperature electronic devices [1]. Thin films of ZnO preferentially oriented along the c-axis have been used as surface acoustic wave (SAW) devices because of their large piezoelectric constant [9].

ZnO is transparent in the visible light range, operating in the UV to blue wave-

lengths as indicated by its direct bandgap energy of 3.3 eV. This makes ZnO a promising material for applications in transparent electronics, optoelectronics and spintronic devices [1].

Indium tin oxide (ITO) is currently being used to great effect in these kinds of applications, with existing technology based on In_2O_3 films being well utilized. However there is price volatility associated with indium, along with various supply concerns, which have pushed forward the need for the development of ITO substitutes [10]. Owing to better stability in hydrogen plasma when compared with ITO, zinc oxide thin films can be used in the fabrication of hydrogenated amorphous silicon solar cells [11]. Zinc is also cheap and abundant and shows low toxicity. With thin films of ZnO easily grown at relatively low temperatures, and on inexpensive substrates e.g. glass [1], doped ZnO is a favoured candidate to replace indium tin oxide (ITO) based TCO films.

Zinc oxide is widely used in non-electronic applications too, such as in white paints, and as an additive which provides UV stability to plastics. It is used for activation of the vulcanisation process in rubber, in catalysis, and in pharmaceuticals and cosmetics for sun protection [2].

ZnO forms a wide range of nanostructures including sheets, rods, flowers, and stars. These structures are ideal for detection applications due to the large surface-area to volume ratio [1]. Zinc oxide nanorods can be formed on a wide variety of substrate materials with varying degrees of c-axis orientation. The formation of such structures is dominated by anisotropic growth along this axis as a result of surface energy differences in the highly polar planes of ZnO. The ZnO nanostructure system has been modelled by colleagues at Industrial

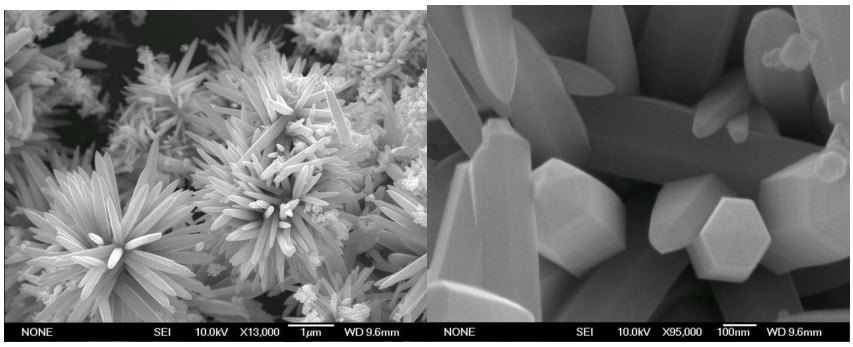

Figure 1.1: SEM micrographs of ZnO crystals

Research Limited using *ab initio* computation techniques [12, 13]. These results indicate that certain crystal facets grow faster than others, leading to the various observed morphologies. Electrochemical deposition of ZnO nanorods has previously been studied using synchrotron radiation, with the effects of deposition times, temperatures and other process parameters reported [14–17].

Zinc oxide occurs in nature as the mineral zincite, which crystallises in the hexagonal wurtzite structure $P6_3mc$. The hexagonal unit cell (a=0.325 nm, c=0.520 nm) contains 2 formula units, where the zinc atoms are surrounded by oxygen atoms in a nearly tetrahedral configuration, as shown in Figure 1.2. Along the c-axis the Zn-O distance is somewhat smaller ($dZn\text{-}O_{[1]} = 0.190nm$) than for the three neighbouring oxygen atoms ($dZn\text{-}O_{[2]}=0.198nm$). When these tetrahedra pack together to form the crystal structure, the resulting coordination gives rise to a polar symmetry along the hexagonal axis of the unit cell. This polarity is responsible for some of the inherent properties of ZnO, namely its piezoelectricity and spontaneous polarisation. It is also important to consider when addressing processes such as crystal growth and the generation of defects within the structure [1]. A metastable cubic phase with the rocksalt (NaCl) structure is also known [2].

It has been established that the n-type conductivity in non-stoichiometric zinc oxide is due to interstitial zinc atoms and/or oxygen vacancies. Since the electrical conductivity of ZnO is directly related to the number of electrons, electrons formed by the ionisation of the interstitial zinc atom and the oxygen vacancies affect the electrical conductivity of ZnO crystals [18].

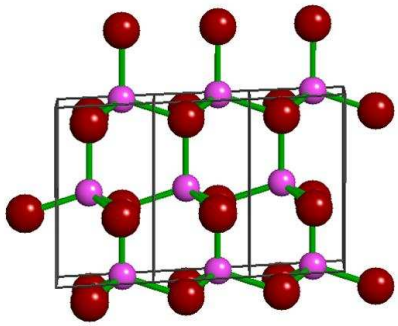

Figure 1.2: Hexagonal wurtzite structure of ZnO

1.2 Doped Zinc Oxide

Thin films of pure ZnO are not stable against corrosive environments e.g. the adsorption of O_2 decreases the electrical conductivity of the film, and also changes the surface morphology. Doping ZnO with different elements has been investigated [19–22] in the hope of making the ZnO system resistant against such changes [23], resulting in an interesting family of materials based on doped ZnO.

A large area of work focused on doped ZnO has investigated the group 13 elements Al, Ga and In [6, 24–29]. These elements can substitute easily for Zn in

the crystal lattice, and this type of doping has been shown to result in high carrier concentrations, >1020 cm^{-3} [24, 30]. In fact, these types of ZnO produce some of the highest-conductivity transparent material available today. Donor type behaviour has also been exhibited by F and Cl [31] which replace oxygen atoms within the lattice. Group 14 elements such as C, Si and Ge have properties which would suggest they could be electrically active as either donors or acceptors, however there is no strong evidence to support this occurring [32].

Recently, ferromagnetism has been induced in ZnO by doping with a transition metal, e.g. Mn. These samples showed practical Curie temperatures, making them suitable for use in spintronic device applications. ZnO also has the coveted ability for bandgap tuning, by way of divalent substitution at the Zn^{2+} site which forms heterostructures. Bandgap energies of ∼3.0 eV have been reported by doping with Cd^{2+}, with Mg^{2+} increasing the bandgap energy to ∼4.0 eV [1].

ZnO typically exhibits n-type conductivity, where the dopants contribute extra electrons, creating an excess of negative charge carriers. The fabrication of p-type ZnO (where the dopant accepts electrons from the host material, leaving positive holes), for use in p-n junction based devices has encountered difficulties due to the self-compensation effect from defects such as interstitial zinc atoms and oxygen vacancies in the native ZnO. Nitrogen is seen as the most promising candidate for successful p-type doping of ZnO films, because of its similar radius to the oxygen atom. Several groups report p-type ZnO:N films made via thermal oxidation of a Zn_3N_2 precursor [33–35], which addresses the problem of the low solubility of N acceptors in ZnO, but the resulting films are not particularly stable, and the mechanism by which N is incorporated is not clear [36].

1.2.1 Incorporation of Al

Of the studies reporting the inclusion of dopant ions, few have convincingly looked at the location of the dopant ions [36, 37]. They may reside totally within the zincite crystals, (substitutionally in the Zn sites), or significant exclusion could occur, leaving the dopant to agglomerate between crystallites. The latter would result in increased inter-grain resistivity, which is undesirable for TCOs. An ability to examine this raises the possibility of improving and optimizing the dopant location through adjusting the different processing parameters such as heating profile, precursor chemistry etc.

A dopant ion introduced to modify the electronic properties of a material needs to be incorporated into the crystal structure of the host material (either in lattice sites or interstitially). In the case of a ZnO:Al TCO, the Al^{3+} ion is required to occupy a Zn^{2+} lattice site in order to provide a free electron (charge carrier) and enhance the conductivity of the ZnO [23]. A simplistic representation is shown in Figure 1.3a, where an Al^{3+} occupies the site of a Zn^{2+}, producing a charged defect [38].

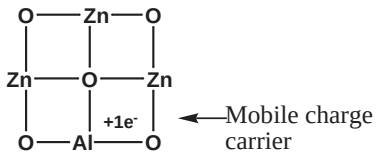

(a) Al^{3+} occupying a Zn^{2+} site

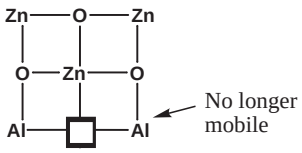

(b) Al^{3+} occupying adjacent sites

Figure 1.3: Possible incorporation sites of Al^{3+} ions into the zincite lattice.

A quantum chemical approach has been applied to the structural, electrical and electronic properties of ZnO due to the Al doping, and explains the increase in the n-type electrical conductivity [39]. In order to attain optimum

performance, the material would be expected to incorporate a uniform and homogeneous distribution of dopant ions in the correct locations, up to a limiting concentration. Too high a concentration could lead to dopant ions occupying adjacent or proximal lattice sites as in Figure 1.3b, causing ion vacancies, resulting in a neutral defect which would not contribute to conductivity [38].

Jimenez-Gonzalez [23] explains the increase in the conductivity of ZnO when Al is introduced as a dopant, in terms of donor behaviour from Al. Because Al has one valence electron more than Zn, substitution of Al for the Zn atom (Figure 1.3), or Al occupation of the interstitial sites increases the concentration of charge carriers present in the material. Al doping of ZnO is favoured by both the small difference in electronegativity values of Zn (1.65) and Al (1.61) and the smaller ionic radii of Al (0.530, 0.675Å) when compared with Zn, (0.60, 0.710Å) in the tetrahedral and octahedral configurations respectively.

Materials produced using lower temperature processes could be in non-equilibrium states. i.e. the Al doping in the tetrahedral Zn sites could simply be the result of kinetic convenience, or alternatively the solubility limits could vary with temperature. On high temperature annealing, the lower solubility of Al in ZnO encourages migration of the Al ions toward the surface forming regions of lower energy compositions. These could be Al-O clusters or amorphous precursors to, for example $ZnAl_2O_4$ [40–42].

In the hexagonal close packed lattice of the ZnO wurtzite structure, half of the tetrahedral holes and all of the octahedral holes are empty, providing further possible dopant sites. The Al^{3+} ion is smaller than the Zn^{2+} ion and could easily be accommodated in either hole, however, taking into account geometry preference rules one would expect a preference of Al for the octahedral hole [43].

Unincorporated dopant could also reside in a non-conductive inter-grain layer resulting in electrical isolation of the individual crystallites. High temperature (>800°C) processing of Al-doped ZnO has previously demonstrated the ready formation of inter-grain impurity phases [42].

In doped ZnO systems, the dopant has been reported to act as an electrical dopant at lower doping concentrations, but as an impurity at higher doping concentrations, which exhibit the lowest electrical resistivities [44].

The importance the dopant ion location has on the optical and electronic properties of ZnO led to an attempt to more accurately track the fate of the Al dopant ions, and to determine whether the proportion that are actually incorporated into the appropriate sites of the crystalline ZnO can be more accurately quantified. An interesting question arises as to whether the conditions for maximum dopant incorporation coincide with those necessary to produce highly oriented thin films [40] and/or whether either of these result in optimum TCO characteristics.

1.3 Preparation Techniques

Doped ZnO as a transparent conducting oxide (TCO) is readily prepared using physical techniques such as vacuum evaporation, sputtering, CVD, etc [8], sol-gel dip coating [9, 23, 39, 45, 46], spray pyrolysis [47], and sol-gel spin coating [11, 18, 26, 48, 49]. This has provided a solid body of knowledge on the material and its properties [2].

Physical deposition methods such as pulsed-laser deposition and RF magnetron sputtering produce films with good electrical and optical properties at lower deposition temperature, however it has the disadvantages of a relatively low deposition rate, and high cost for equipment [44].

1.3.1 Sol-gel Syntheses

The use of wet chemical processing, and sol-gel deposition in particular, offers an alternative to expensive vacuum deposition techniques for producing large area thin film coatings. This may also improve manufacturing throughput since it enables direct patterning, for example using ink-jet printing, micro-contact and reel to reel printing. The sol-gel route has been used for preparing various kinds of functional oxide films (including ZnO) such as TiO_2, $BaTiO_3$, $LiNbO_3$, ITO and $Li_2B_4O_7$ films [9].

A number of studies have examined the influence of processing details (heating profile, temperature, solvents etc) on film properties and performance [38–40, 44, 46, 50–55], however, despite identifying optimum processing conditions, there is limited understanding as to why the processing variables influence electrical properties such as resistivity.

Sol-gel synthesis conditions can be manipulated to ensure the morphology of ZnO thin film is dominated by c-axis growth [9, 18, 39, 44, 48] which has been associated with lower resistivity films. This could however be coincidentally related to other film attributes relating to crystal growth, film density and inter-grain barrier density. It is not clear why an exclusively c-axis aligned film should have lower resistivity than a randomly oriented layer, which may

have better inter-grain connectivity. It has also been found that any preferential orientation of the crystallites is not lost with annealing as it has been in ZnO films prepared by other techniques [56].

While sol-gel film preparation has been proposed as a cheap, scalable process suitable for commercialisation, the necessity to apply multiple layers to achieve the required conductivities remains a weakness.

1.4 Thin Films

The thin films fabricated and characterised in this work are spin-coated, with sol-gel deposition from organically modified precursor solutions. This method was designed to deposit active films in a single coat. Films incorporating 1–2 atom% of a dopant such as Al have been shown to result in low resistivity materials while retaining high transparency [52, 57–61], the two main properties of a TCO. This was aimed at developing an understanding of the effect of process parameters on the dopant incorporation, and how the presence of dopant ion affects the nucleation and growth of the ZnO crystallites. This will allow the deposition conditions to be fully controlled, in order to optimize the properties of the thin films.

Previous studies have shown, that the surface texture and resistivity of solution derived films are sensitive to the concentration of the sol-gel solution [50] as well as the heating profile(s) used to calcine the films [51, 52]. Rapid thermal annealing appears to result in highly (002) oriented films [52, 53] with low resistivities, agreeing with other observations that higher conductivities and transmittances occur in films with preferential c-axis orientation [44] while

other studies appear to suggest more random orientations are preferred [54]. Preferential orientation of the crystallites is believed to be a result of at least two physical conditions of the gel-film: the internal stress and surface energy [11].

There is general agreement that ZnO : Al TCOs with low resistivities appear to require around 1 atom% added Al dopant, and post-synthesis annealing at *ca* 400-500°C [44,46,53–55]. However, lattice deformation measurements made to attempt to quantify the effective dopant concentration suggest that the effective Al concentration is much lower than the added Al concentration [46].

The n-type conductivity shown by non-stoichiometric ZnO is known to be a result of interstitial Zn atoms and oxygen vacancies within the crystal structure [62], and as such, additional electrons formed by the ionisation of interstitial zinc atoms, or resulting from the oxygen vacancies, affect the electrical conductivity of ZnO. These defects are thought to be responsible for the noted decrease in the resistivity of films heated in a reducing atmosphere post-annealing, as has been widely reported [30,55,58,61]. A second annealing step in a reducing atmosphere increases the number of oxygen vacancies, and may also increase the carrier concentration in the film by releasing carriers trapped in the grain boundaries via oxygen annihilation from the ZnO crystals [63].

1.4.1 Thin Film Solar Cells

Thin film solar cells show great potential in the continuing development of photovoltaic energy conversion. The thin film components are produced using highly favourable methods in terms of the amount and expense of raw materials

used, the simplicity of processing which occurs at relatively low temperatures, and the ability to deposit films over large areas with little complication. Only a few micrometers of film thickness is needed to absorb most of the sunlight required for the film to be effective, and the energy saved during production processes contributes to shorter energy pay-back times.

A transparent window electrode is needed to allow the transmission of light through the cell and extraction of the photocurrent. Amorphous silicon [64] and Cu(In,Ga)(S,Se)$_2$ [65,66] cells make particular use of ZnO containing high levels of dopant. The incorporation of high levels of trivalent dopants such as Al, B or Ga contribute to films which exhibit carrier concentrations up to 1.5x10 ^{21}cm^{-3} and resistivities as low as 2x10^{-4} Ωcm.

The transparent electrode in amorphous silicon cells is degenerately n-doped. A tunnel junction is formed between the electrode and a highly p- or n- doped material, while ZnO is a part of the electric p/n junction in Cu(In,Ga)(S,Se)$_2$ cells. A bilayer structure consisting of a thin (∼50nm) nominally undoped ZnO layer and a highly n-doped layer is typically used to obtain high efficiencies. The ZnO films predominantly act as a transparent conductive front contact of the cell, but can also contribute to optical functions such as the scattering and trapping of light, and enhancing the reflection of light at the back contact surface of the cell [2].

Improvements to the optical and electronic properties of ZnO thin films holds great promise in obtaining higher conversion efficiencies in thin film solar cells. This makes them a more viable option, both technically and financially, as a sustainable energy source.

Chapter 2

Characterisation

The formation of doped ZnO materials using a modified sol-gel technique, and the assessment of the influence of the precursor solution, the thermal processing and the dopant concentration on the material was investigated using X-ray diffraction (XRD), scanning electron microscopy (SEM) and solid state nuclear magnetic resonance spinning at the magic angle (MAS NMR). The influence of dopant concentration on the crystallite sizes and unit cell dimensions was also examined using XRD Rietveld analysis.

2.1 Solid State ^{27}Al NMR

Magic angle spinning (MAS) is the most commonly used technique in solid state NMR experiments. It is a method of obtaining highly resolved spectra for nuclei such as ^{27}Al, where the signal in the solid state powder spectra is broadened significantly by the electric quadrupole interactions of the spin, I=5/2 nuclei [67]. ^{27}Al has 100% natural abundance, and a fast relaxation time allowing many pulses to be collected for samples with low Al concentrations, which is necessary in obtaining a useful and representative spectrum. Collect-

ing more scans for each sample also reduces the signal to noise ratio, reducing the background noise which can obscure spectra if left too high. The main use of aluminium NMR is to detect the presence of aluminium and measure its relaxation rate in order to determine coordination arrangements and site occupancy within the different binding sites of the sample. The width of the ^{27}Al signal increases with the asymmetry of its environment.

In a MAS experiment, the sample is spun at high speed (in this case, 10–12 kHz) at an angle of 54.74° with respect to the magnetic field direction. This is known as the magic angle. Away from this angle, only sidebands from second-order broadening of the central transition can be seen. As the magic angle is approached, the sidebands from the satellite transitions are observed, and become progressively narrower. In this way, MAS allows the NMR spectrum to be narrowed into a visible set of sidebands over a limited but not too restrictive range of angles about the magic value [68].

^{27}Al NMR has previously been used to examine the limits of solid solution of Al in ZnO [38, 69]. This showed a very low (<0.005) Al solubility, however these studies were carried out on materials subjected to high temperature annealing (850–1100°C), far in excess of temperatures used to produce low resistivity Al-doped conductors [9, 11, 18, 23, 39, 44, 46, 48, 50–55].

Octahedrally coordinated Al is generally observed at 0±15 ppm, while tetrahedral Al is seen at 65±15 ppm [68]. The spectra observed for these samples include a narrow signal at *ca* 81.2 ppm, (tetrahedral) and a much broader signal centred at 8.2 ppm (octahedral). A less intense, although broad signal also appears centred at 75 ppm (tetrahedral).

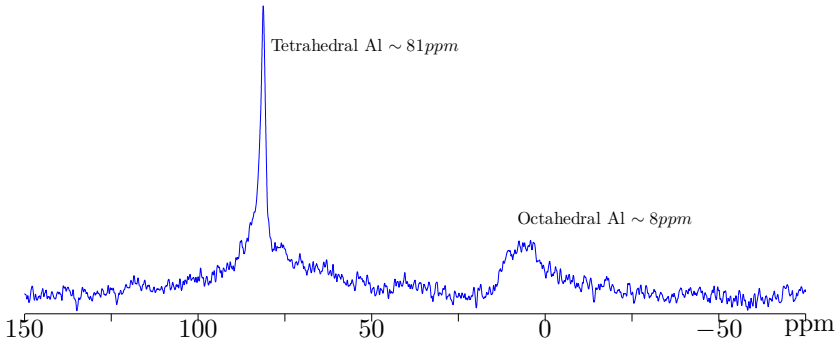

Figure 2.1: ^{27}Al NMR spectrum of a typical ZnO:Al sample containing 2 atom% aluminium.

The integration of solid state ^{27}Al NMR signals does not provide reliable quantitative data on the relative abundance of each signal type, but the change in relative intensities between the different signals could be used to provide a semi-quantitative estimate of the relative Al site occupations of the samples.

The narrow signal observed at *ca* 81.2 ppm does not appear to exhibit a quadrupolar line shape. It is indicative of Al in a highly symmetrical tetrahedral environment, and is likely to correspond to Al located in isolated Zn^{2+} sites of crystalline ZnO. The line width varies slightly between samples, but it could be supposed that this Al is subject to a high degree of local ordering such as that proposed in Figure 1.3a having no other dopant ions in the immediate vicinity, and no adjacent vacancies. The signal is at much lower field than is normally observed for Al oxides [68], which could reflect the local charge density or field strength due to being surrounded by four tetrahedral Zn^{2+} ions in comparison with more highly charged ions such as other Al^{3+} ions in (e.g. in γ-alumina) or Si^{4+} ions as seen in framework aluminosilicas [68].

Also of interest is a recent study showing ^{27}Al NMR of Al located in the octa-

hedral Ti sites in crystalline Al doped rutile [70]. This appears at higher field (δ_{iso} = -5 ppm) than the octahedral γ-alumina signal (14.7 ppm) and exhibits a narrow quadrupolar line shape.

Solid state ^{27}Al MAS NMR data were collected at 11.7 T (Bruker Avance 500 spectrometer with 4 mm Doty MAS probe spun at 10-12 kHz). Spectra were acquired at 130.245 MHz using a 15° pulse of 1 s and a recycle time of 1s, and referenced to $Al(H_2O)_6^{3+}$.

2.2 X-Ray Diffraction

Powders

ZnO:Al powders were characterised using XRD in order to determine the crystallisation temperature of ZnO, both with and without aluminium, as well as any effects the amount of aluminium or the different heat treatments had on the composition and crystallinity of the samples. A zincite phase was almost exclusively present in all samples, apart from one containing 8 atom% Al, heated to 800°C. This sample showed both zincite (ZnO) and gahnite ($ZnAl_2O_4$/$ZnO.Al_2O_3$) phases.

Data for all powder samples were collected on a Philips PW3700 series diffractometer using Co-Kα radiation.

Quantitative Analyses

XRD data were collected on a range of ZnO powders with differing Al contents in order to accurately calculate the unit cell dimensions, and the changes

in these due to doping. Rietveld analysis was used in order to investigate the changes in lattice parameters as a function of the Al concentration, by way of optimising the fit between the XRD data obtained and the computed model pattern for ZnO with a least squares approach. A disadvantage of using this technique is that many parameters must be fit to the data set, including background, peak shape and structural parameters. ZnO displays elongated crystallites (Figure 1.1). Because of this, two size modes were required to model the full width at half maximum (FWHM) variations, because of reflections comprised of the different contributions of c- and a-axis geometry.
The crystallite sizes and unit cell dimensions of the zincite formed were determined using TOPAS XRD software.

Films

ZnO:Al films were studied using XRD to determine their crystal orientations. It has been previously reported [58] that films with preferential 002 (c-axis) orientation show the lowest resistivities. It was found that by modifying the thermal processing route used, the crystal orientation (with regard to preferential crystallite orientation) could be easily controlled.
Crystallinity and crystal orientation of films were examined using D8-AVANCE diffractometer using Co Kα radiation.

2.3 Scanning Electron Microscopy

SEM was used to obtain images of the surface morphology and relative crystallite sizes of ZnO powders containing different amounts of Al. It was observed that as the Al content of samples increased, the crystallite sizes decreased. This is the same trend as was found in the XRD data. The accumulation of

Al at the inter-grain boundaries is also noticeable, with this seen to increase with higher Al concentrations.

SEM imaging was performed on a JEOL JSM-6500F field-emission scanning electron microscope. Samples were deposited onto a Si wafer and coated with 10 nm of Pt in a JEOL JFC-1500 ion sputtering device. Standard SEI digital images were obtained at an accelerating voltage of 10-15 kV and viewed at a working distance of 9-11 mm.

2.4 UV-Vis Transparency Measurements

Measurements were taken of thin films on quartz substrates, using a Hewlett Packard 84524 diode array spectrophotometer. These were recorded over the range of 200-800 nm. Disruptions in the spectra, most noticeably around 650 nm are due to diffraction grating changes and should be ignored. All spectra show a sharp absorption edge at around 380 nm, corresponding to the band gap of ZnO. The weak fluctuation in the transmission spectrum has been observed by others [11], and is due to interferences in the thin film from the air-ZnO and ZnO-quartz interfaces producing reflections.

2.5 Differential Scanning Calorimetry & Thermogravimetric Analysis (DSC–TGA)

Differential Scanning Calorimetry (DSC) measures the temperature and corresponding heat flows which result from phase transitions occurring in a material, as it is heated. The information provided by this technique allows the identi-

fication of endothermic (such as melting) and exothermic (i.e. crystallisation) processes, and the temperature or applied energy at which these take place.

Thermogravimetric analysis (TGA) measures the change in mass of a sample as a function of temperature. It can identify temperatures of phase changes and reactions, and is helpful in determining the composition of both a starting material and its decomposition products.

The two analytical methods were run together, using the same instrument, and give insight into the physical and/or chemical changes which occur during the crystallisation of ZnO from aminoalcohol containing sol-gel solutions.

Thermal analysis was carried out on samples pre-dried at 90°C. Data were collected using an Alphatech SDT Q600 thermo-analyser under flowing air (50mL min^{-1}) at a heating rate of 10°C min^{-1}.

2.6 Film Thickness Measurements

A DekTak profilometer was used to give a surface profile of the thin films, providing information on the roughness of the films, as well as giving an indication of the film thickness. This was achieved by removing a section of the film from the substrate (either physically, with a scalpel blade, or chemically, by masking off a section of the films and removing the exposed film in HCl), and then measuring the difference in vertical height between the coated and uncoated parts of the substrate.

The profilometer works by moving a small stylus over the surface of the film, with variations in its vertical height transmitted as a digital signal, giving a

step-like pattern corresponding to the surface of the film, as shown below;

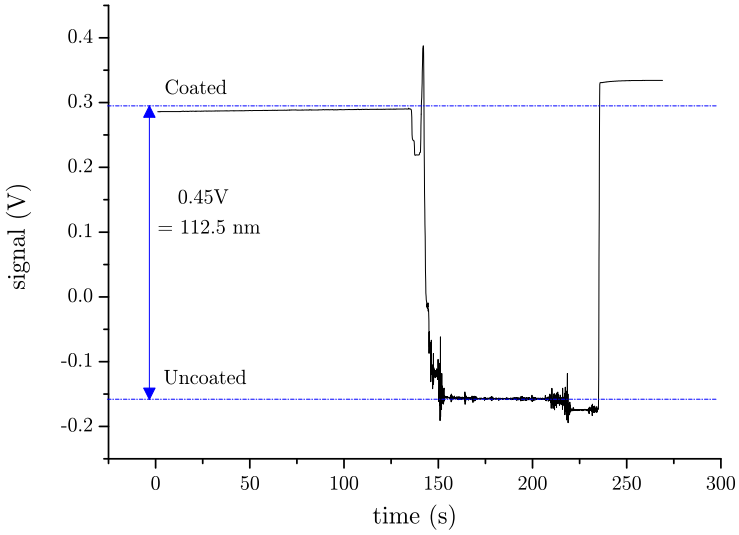

Figure 2.2: Surface profile of a typical ZnO:Al film.

2.7 Resistivity Measurements

A 4–point probe utilizing the Hall Effect was used to measure the resistivity of the thin films. The Hall effect is the production of a voltage difference (the Hall voltage) across an electrical conductor (in this case the ZnO:Al film), which is transverse in direction to an electric current in the conductor and a magnetic field perpendicular to the current [71].

When no magnetic field is present, distribution of the current is uniform and no potential difference is seen across the output. When a perpendicular magnetic field is present, a Lorentz force is exerted on the current. This force disturbs the current distribution, resulting in a potential difference (voltage) across the output. This voltage is the Hall voltage (VH).

$$V_H \propto I \times B \tag{2.1}$$

The van der Pauw Method is a commonly used technique for measuring the resistivity of a sample. It is widely applicable as it allows the properties of a sample of any arbitrary shape to be accurately measured. The only stipulations are that the sample must be approximately two-dimensional i.e.. it is much thinner than it is wide, and that the electrodes are placed on its perimeter. From these measurements, electronic properties of the material such as resistivity, carrier mobility and doping type (p-type of n-type) can be determined [72].

Sample preparation

The thickness of the sample to be characterised must be much smaller than its width and length in order to use the van der Pauw method. Symmetry of the sample is desirable in reducing any calculation errors, and there cannot be any isolated holes in the sample in order to obtain accurate results.

To carry out the measurements, four ohmic contacts are placed on the sample. These contacts must be positioned on the edges of the sample, or as close to this as is possible, and must be as small as possible - in calculations they are regarded as being infinitely small. Any errors associated with their non-zero size will be of the order D/L, where D is the average diameter of the contact and L is the distance between the contacts.To reduce any errors introduced by thermoelectric effects, the four contacts should be made of the same material, and any leads running from the contacts should be made from the same batch of wire.

Measurement Definitions

- The contacts are numbered from 1 to 4 in a counter-clockwise order, beginning at the top-left contact.

- The current I_{12} is a positive DC current injected into contact 1 and taken out of contact 2, and is measured in amperes (A).

- The voltage V_{34} is a DC voltage measured between contacts 3 and 4 with no externally applied magnetic field, measured in volts (V).

- The sheet resistance R_S is measured in ohms (Ω).

Basic measurements

For each measurement, a current is applied along one edge of the sample (for instance, I_{12}) and the voltage across the opposite edge (in this case, V_{34}) is measured. From these two values, a resistance (for this example, $R_{12,34}$) can be found using Ohm's law:

$$R_{12,34} = \frac{V_{34}}{I_{12}} \tag{2.2}$$

Van der Pauw found that the sheet resistance of samples can be calculated from two of these resistances - one from along a vertical edge, such as $R_{12,34}$, and a another measured along a horizontal edge, such as $R_{23,41}$. The sheet resistance is related to these by the van der Pauw formula;

$$e^{-\pi R_{12,34}/R_s} + e^{-\pi R_{23,41}/R_s} = 1 \tag{2.3}$$

Reciprocal measurements

The reciprocity theorem [72] states that;

$R_{AB,CD} = R_{CD,AB}$

So a more precise value of the resistances $R_{12,34}$ and $R_{23,41}$ can be found by taking measurements of their reciprocal values $R_{34,12}$ and $R_{41,23}$ and averaging the results.

If;

$$R_{\text{vertical}} = \frac{R_{12,34} + R_{34,12}}{2} \tag{2.4}$$

and

$$R_{\text{horizontal}} = \frac{R_{23,41} + R_{41,23}}{2} \tag{2.5}$$

Then, the van der Pauw formula becomes

$$e^{-\pi R_{\text{vertical}}/R_S} + e^{-\pi R_{\text{horizontal}}/R_S} = 1 \tag{2.6}$$

Reversed Polarity Measurements

Repeating the resistance measurements after switching the polarities of both the current source and the voltage meter leads to more accurate determination of the resistance values. As the same area of the sample is being measured, but in the opposite direction, the values of $R_{vertical}$ and $R_{horizontal}$ can still be calculated as the averages of the standard and reversed polarity measurements, and by doing this, any offset voltages, such as thermoelectric potentials due to the Seebeck effect, will be cancelled out.

Combining these measurements with the reciprocal measurements from above gives;

$$R_{\text{vertical}} = \frac{R_{12,34} + R_{34,12} + R_{21,43} + R_{43,21}}{4} \tag{2.7}$$

and

$$R_{\text{horizontal}} = \frac{R_{23,41} + R_{41,23} + R_{32,14} + R_{14,32}}{4} \tag{2.8}$$

Measurement accuracy

The reciprocal and reversed polarity measurements both serve to check the repeatability of the results. The reversed polarity measurements should agree to within 3% of the corresponding standard polarity results, with the same agreement needed between the reciprocal measurements. Any significant disagreement in values could be due to a source of error within the setup, and should be addressed in order to gain meaningful results.

Calculating sheet resistance

In general terms, the rearrangement of the van der Pauw equation to give the sheet resistance R_S in terms of known functions is not possible, unless $R_{vertical} = R = R_{horizontal}$; in this case the sheet resistance would be given by;

$$R_s = \frac{\pi R}{\ln 2} \tag{2.9}$$

2.8 Reagents

These reagents were used in all following syntheses; Zinc Acetate dihydrate, Scharlau

Aluminium sec-butoxide, Sigma

Citric acid monohydrate, Scharlau

Citric acid (anhydrous), Scharlau

Methyl diethanolamine, Acros

Diethanolamine, Acros

2-aminoethoxyethanol, Acros

3-amino-1-propanol, Acros

Ethanolamine, Acros

Polyoxyethylene 10-oleoyl ether (Brij 97), Sigma

Chapter 3

Bulk Powders

3.1 Sol-gel synthesis

A previous synthesis route [73] has been adapted with the eventual aim of creating thicker films with fewer layers required, making the spin-coating process more efficient. This route was derived from the Pechini method [74] whereby citric acid is co-polymerized with glycol, glycerol or aminodiols [75].

Al-doped zinc oxide powders were made via a sol-gel method, where zinc citrate was prepared from the reaction of aqueous zinc acetate with 1 molar equivalent of citric acid. The liberated acetic acid was removed by rotary evaporation to dryness at 80°C, followed by re-suspending the residue in distilled water and repeating to remove any further acetic acid. Two molar equivalents of an aminoalcohol chosen from methyl diethanolamine (MDEA), diethanolamine (DEA), aminoethoxyethanol (AEE), 1-amino-3-propanol (PA), and ethanolamine (EA), were added to the citrate to solubilise the Zn citrate salt in water.

An aluminium citrate solution was prepared from aluminium sec-butoxide and

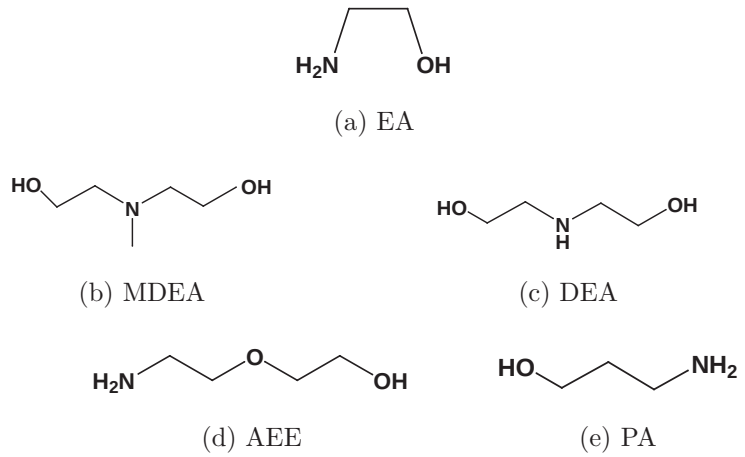

(a) EA

(b) MDEA

(c) DEA

(d) AEE

(e) PA

Figure 3.1: Structures of the different aminoalcohols used; ethanolamine(EA), methyl diethanolamine(MDEA), diethanolamine(DEA), 2-amino ethoxyethanol(AEE), 3-amino-1-propanol(PA).

anhydrous citric acid (1:1 ratio) in iso-propanol. Removal of the solvents was carried out by rotary evaporation, and the solid residue was redissolved in distilled water to prepare a standard solution. This was added to the Zn solutions to form mixtures containing Al in concentrations of 0, 1, 2, 4, 8 atom% with respect to Zn. The Zn concentration of the solutions was standardized at 0.5 mol L^{-1}. Aliquots of the solutions were placed in shallow crucibles and thermally processed via gelation and calcination to form ZnO:Al powders.

A preliminary drying step carried out at between 70-160°C in an oven was followed by heating in air in a furnace up to 500°C, either at 5°C min^{-1} heating rate and held for 1 hour (*Slow* heating profile), or by placing in a preheated oven at 500°C and held for 1 hour (*Fast* heating profile). Selected samples were further annealed at 400, 500, or 600°C under vacuum.

Powders were then characterised by solid state ^{27}Al NMR, to determine the end position of the Al, and the relative distribution of the dopant over the

main coordination environments.

3.2 Influence of Aminoalcohol

A series of samples containing different aminoalcohols were prepared in order to determine the effect (if any) this had on the end position of the dopant Al^{3+} ions within the ZnO structure. It was thought that the differing denticity of the aminoalcohols could alter the coordination of the Al^{3+} ions in such a way that the amount of Al incorporated into the ZnO structure could be optimised by selecting the appropriate aminoalcohol. Structures are shown in Figure 3.1.

It was previously reported [9] that the aminoalcohol used (EA or DEA) in the precursor solution had a significant impact on the crystallite orientation of the resulting thin film. The proportion of aminoalcohol present in the sol-gel was also thought to be important, with at least 2 molar equivalents (with respect to Zn) required for the aqueous zinc citrate to dissolve.

Ohyama reported that the use of 2-methoxyethanol and EA, solvents with high boiling points, resulted in transparent ZnO films with strongly preferred orientation [9] and that better electrical and optical properties had been obtained in 0.5 atom% aluminium doped ZnO thin films heated in a reducing atmosphere [58].

Samples containing between 2 and 2.2 molar equivalents of each of the aminoalcohols were investigated, and showed a slightly improved proportion of tetrahedrally coordinated Al up to the 2.1 molar equivalent limit, at which point any more of an excess had little effect, as shown in Figure 3.3. This trend held

for all of the aminoalcohols used.

The ^{27}Al NMR of samples containing 2 atom% Al synthesized using aminoalcohols EA, PA, AEE, DEA and MDEA are shown in Figure 3.2. These samples were dried at 90°C prior to calcination in a 500°C preheated furnace. The spectra all exhibit a narrow signal at *ca* 81.2 ppm, indicative of the tetrahedrally coordinated Al, as well as broader signals centred at 75 ppm (partially obscured by the tetrahedral peak) and at 8.2 ppm (octahedral). The relative proportions of these signals vary significantly for each aminoalcohol. The sample showing the largest proportion of the tetrahedral signal and the smallest of octahedral was that containing EA. This suggested that using this aminoalcohol results in the highest level of dopant substitution into the Zn lattice sites. Because of this, EA was used in all subsequent work.

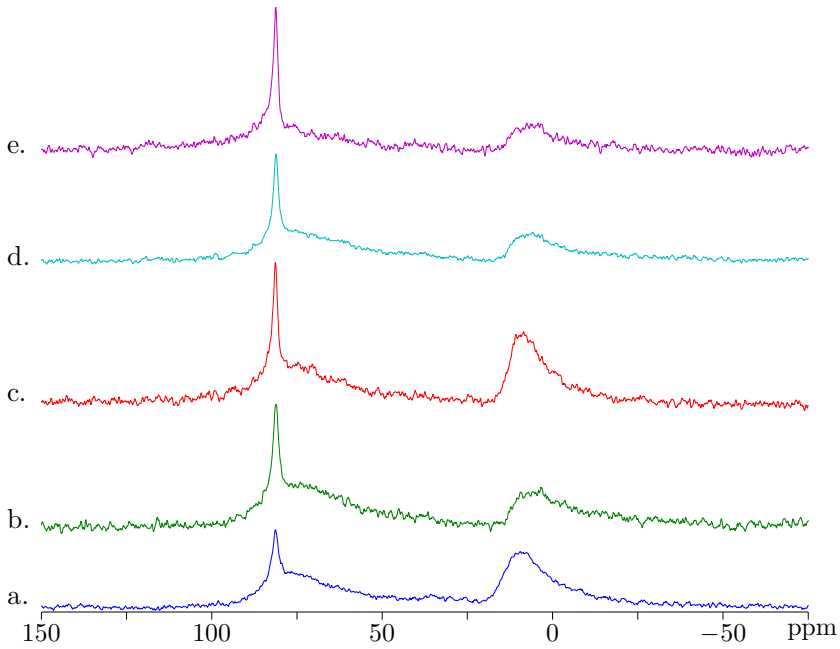

Figure 3.2: The ^{27}Al NMR spectra of samples made with a) MDEA, b) PA c) AEE, d) DEA, e) EA.

There are two possible ways for EA, a bidentate ligand, to coordinate to the zinc atoms; one is to act as a chelating ligand, and the other is to bridge two zinc atoms [9]. EA acts as a complexing agent, also retarding Zn(II) condensation. However, the presence of this amine also increases the pH, which should promote the formation of ZnO [48].

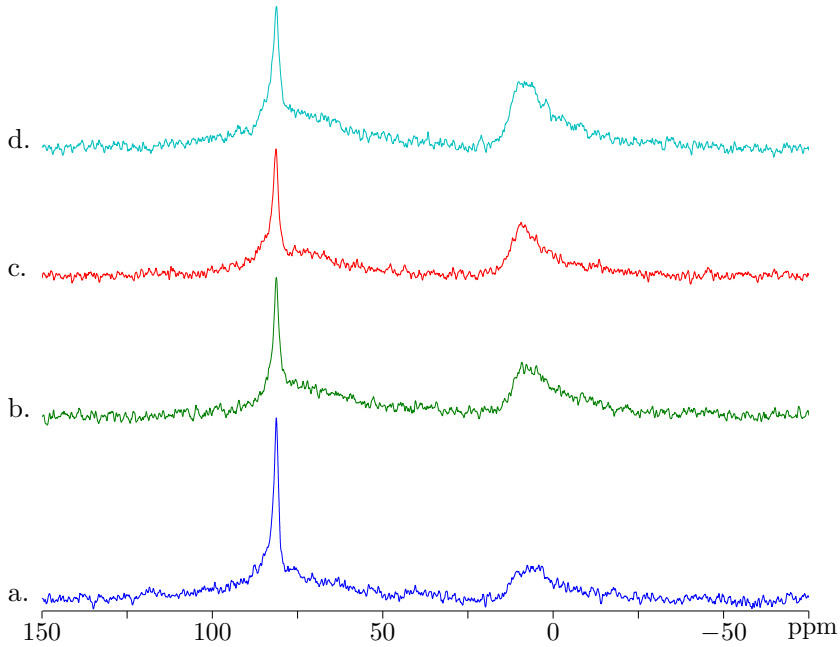

Figure 3.3: The ^{27}Al NMR spectra of samples containing 2 atom% Al and EA at different mole equivalents; a) 2, b) 2.05 c) 2.1 and d) 2.15

Materials prepared with DEA (b.p. 270°C) have been seen to contain organic species after crystallisation had occurred, as a result of incomplete combustion. The presence of these impurities served to inhibit the preferred crystallite growth along the c-axis perpendicular to the substrate, which is undesirable [9].

Although it is difficult to draw a direct relationship with the chemical nature and the relative NMR response, it would appear that generally the higher boiling aminoalcohols result in a less selective speciation of Al ions. It can

Aminoalcohol	Formula	Boiling Point (°C)
N-methyl-diethanolamine	$CH_3N(C_2H_4OH)_2$	247
2-(2-amino ethoxy) ethanol	$C_4H_{11}NO_2$	223
Diethanolamine	$HN(CH_2CH_2OH)_2$	217
Ethanolamine	C_2H_7NO	170
1-Amino-2-propanol	C_3H_9NO	160

Table 3.1: Boiling point data for a range of aminoalcohols

be expected that the structure of the alkanolamine-zinc acetate complexes formed in the sol-gels is somewhat different between the different aminoalcohols, which can be explained by their differing functionalities [9]. A higher boiling aminoalcohol would presumably allow some decomposition of the Zn complex and facilitate mobility of the metal ions during heating, before the organic components are completely removed. In this way, nucleation and selective crystallization of the ZnO could occur.

3.3 Thermal Processing

Effect of Heating Profile

To achieve fully reproducible results, it was observed that heating profiles must be followed very precisely. Samples were all prepared using EA. The sol-gels were dried in an oven at 90°C followed by rapid calcination in a furnace preheated to 500°C. This treatment resulted in much lower intensities of the broader NMR signals, indicating a higher proportion of tetrahedrally coordinated Al compared with samples that were heated slowly in a furnace

to 500°C from room temperature at a rate of 2°C min^{-1} (Figure 3.4).

It appears that a slow heating rate means the crystallization of the ZnO occurs slowly enough to exclude excess impurity ions, resulting in much broader NMR signals, and accordingly, lower levels of overall Al incorporation. When annealed rapidly, kinetics are able to dominate, trapping Al ions in the ZnO lattice, resulting in a non-equilibrium concentration.

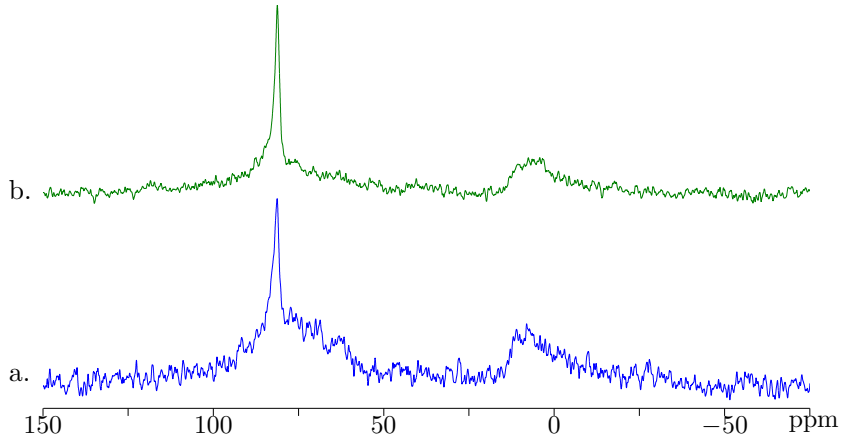

Figure 3.4: ^{27}Al NMR of samples containing EA and 2 atom% Al annealed at 500°C via a) from room temperature at 2°C min^{-1} and b) in a preheated furnace.

Interestingly, samples held at intermediate temperatures (160, 250°C) prior to full calcination at 500°C, also resulted in a less intense 81.2 ppm signal when compared with samples dried below 100°C then subjected to rapid calcination at 500°C (Figure 3.5).

Although not observable in the ^{27}Al NMR or XRD spectra, there is an implication that some nucleation is occurring even as low as 160°C. The mobility of chemical species in the films heated at 160°C, for example, allow a solvolysis

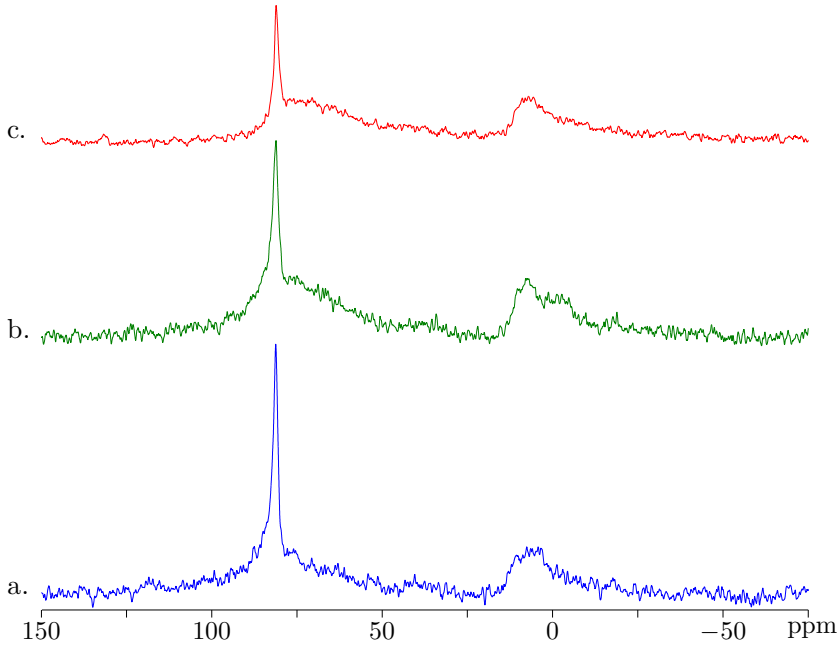

Figure 3.5: ^{27}Al NMR of samples containing EA and 2 atom% Al pre-heated at a) 90°C, b) 160°C d) 250°C before calcination at 500°C.

and condensation crystal growth mechanism to influence crystallisation behavior prior to the slower solid state migration of metal ions after the solvents and organic content of the precursor has combusted or decomposed. To test this hypothesis, the syntheses were repeated with sol-gels containing 40% v/v glycerol heated from room temperature at 5°C min^{-1}, with a 1 hour dwell time at 160°C. The ^{27}Al NMR spectra of these samples showed exclusively octahedral aluminium (Figure 3.6). This is an important result, as an intermediate heating step is often used in sol-gel formation of ZnO films [18, 40, 44, 52–54]. In the case of the citrate based sol-gels at least, this heating profile now looks to be detrimental to the doping efficiency.

The differential scanning calorimetric (DSC) and thermogravimetric (TG) curves of a dried Zn(citrate).2EA solution is shown in Figure 3.7. Oven drying at 90°C overnight removed all of the water and one mole equivalent of

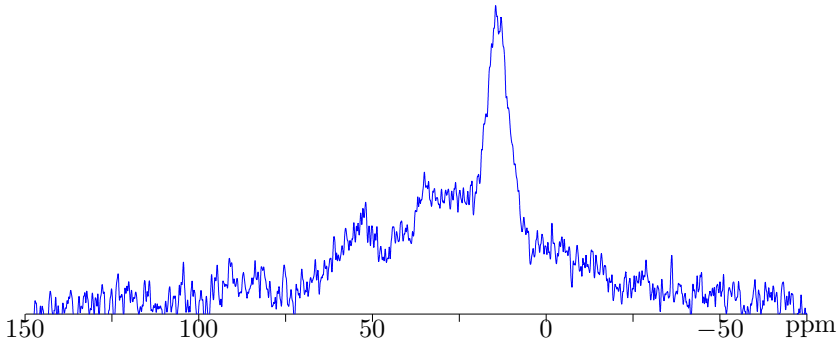

Figure 3.6: ^{27}Al NMR of ZnO:Al with 2 atom% Al and 40% v/v glycerol, displaying almost exclusively octahedral Al coordination.

the EA, leaving a Zn-citrate-EA gel. Thermal decomposition of the residue occurred in three main events; firstly at 210°C, an endothermic weight loss consistent with the dehydration and transformation of the citrate to itaconate [76] occurred with loss of H_2O and CO_2. The exothermic decomposition and combustion of the complex occurred in 2 steps, with an initial onset at 350°C, and a second event beginning at 425°C. The combustion is fully completed by around 500°C, leaving crystalline ZnO. The weight loss from 250-600°C is 73.9%, which corresponds to the theoretical weight loss of 74.3% in the case of complete conversion of Zn(citrate).EA to ZnO.

In order to further examine the differences in materials prepared using different heating rates, a sequence of annealed samples quenched at intermediate temperatures were prepared containing 2 atom% Al. XRD shows that onset of ZnO crystallisation occurs above 325°C (Figure 3.8). This parallels the NMR data which showed that for samples heated rapidly to a range of intermediate temperatures after drying at 90°C, the onset of tetrahedral Al formation begins below 350°C (Figure 3.9).

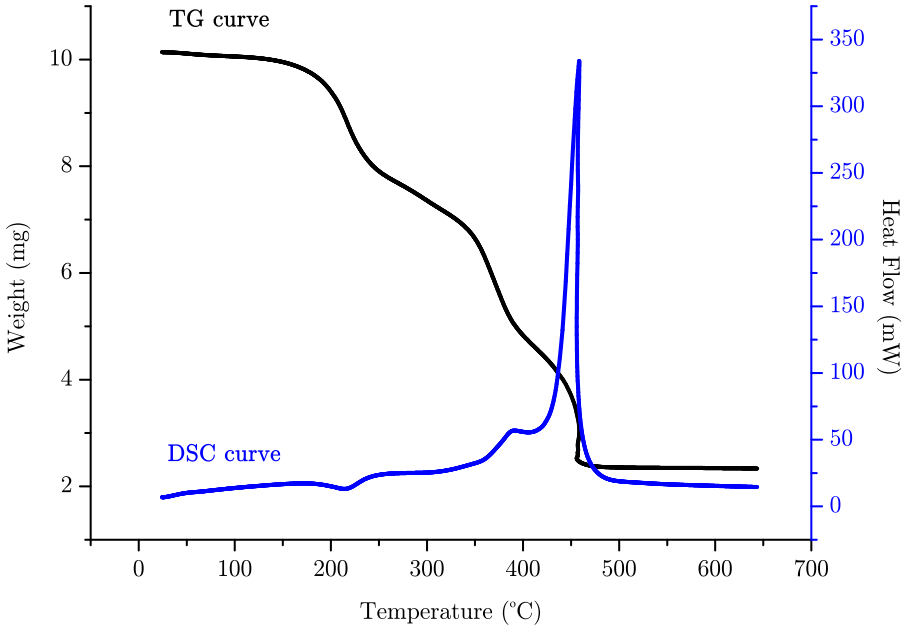

Figure 3.7: DSC-TG analysis of sol-gel derived ZnO, pre-dried at 90°C.

Comparing the XRD data with the TG data, it is seen that some ZnO begins to crystallise as soon as the combustion step commences. This could be a crucial observation when the events leading up to nucleation and crystal growth are considered. The observations do not significantly differ from previous XRD studies of Zn acetate-aminoalcohol studies [9].

Effect of Calcination Temperature

It is apparent from Figure 3.10 that even using optimum processing conditions, a material containing only 1 atom% added Al still contains some Al that is not

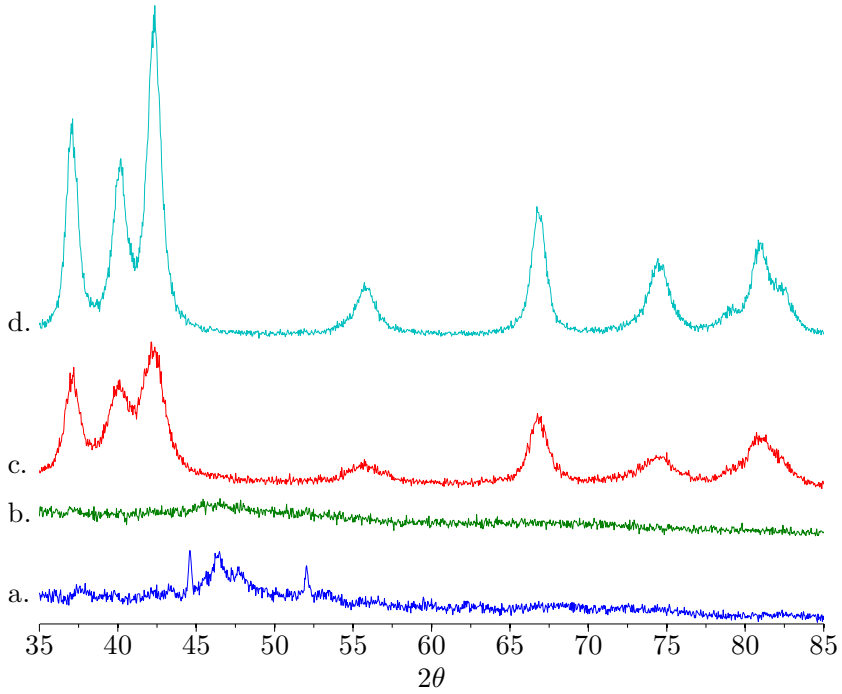

Figure 3.8: XRD traces of ZnO heated at a) 200°C, b) 300°C, c) 350°C, d) 400°C

in the Zn sites of the zincite crystal form. Heating the samples at a higher temperature (600°C) reduces the relative proportion of tetrahedrally coordinated Al and broadens the sharp NMR signal at 82 ppm (Figure 3.11). At these higher temperatures oxygen vacancies can occur, reducing the symmetry of the Al dopant ions, which resulting in more pentacoordinate Al. The presence of such crystalline defects is likely to assist the migration of Al ions, possibly toward the surface which would be more thermodynamically favourable if the concentration of Al ions in the ZnO crystal sites is above the solubility limit [38].

A sample of 8 atom% Al-doped ZnO was heated to 800°C resulting in the crystallisation of a minor $ZnAl_2O_4$ phase (Figure 3.12). This has been observed previously [38, 69] and has been shown to occur at the ZnO grain boundaries

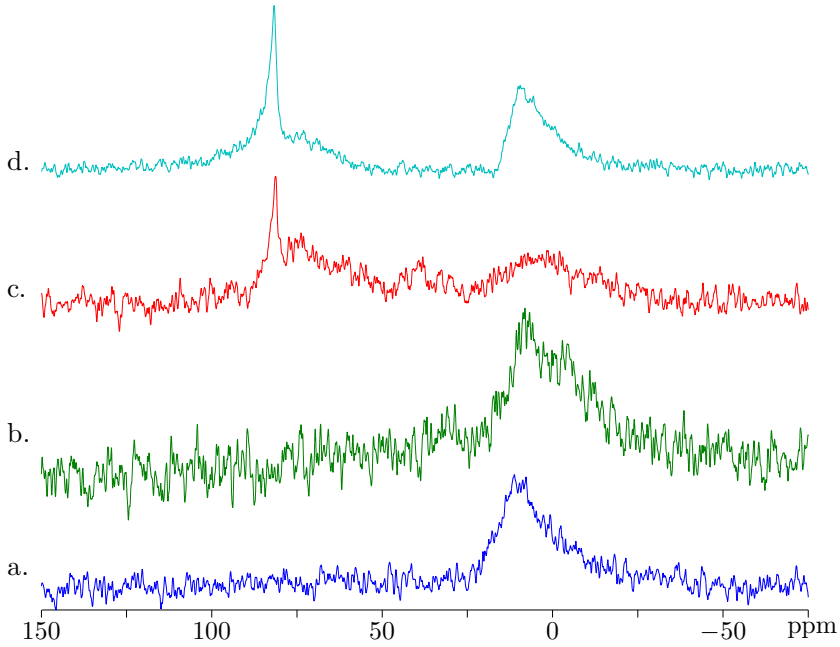

Figure 3.9: ^{27}Al NMR spectra of ZnO heated at a) 200°C, b) 300°C, c) 350°C, d) 400°C.

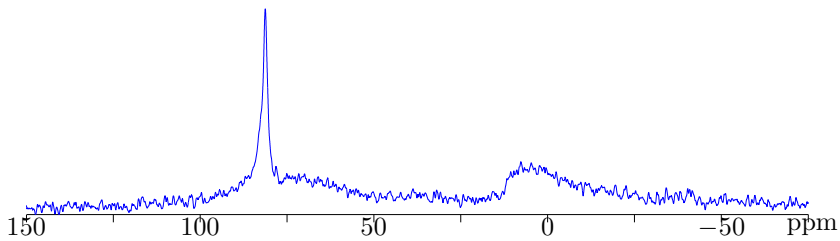

Figure 3.10: ^{27}Al NMR of ZnO with 1 atom% Al, dried at 90°C then annealed at 500°C in a preheated furnace.

[42].

Vacuum Annealing

Annealing the doped ZnO sample under vacuum is expected to increase the concentration of oxygen vacancies in the zincite structure. This allows Zn ions to occupy interstitial sites, producing more free carriers in the material, pro-

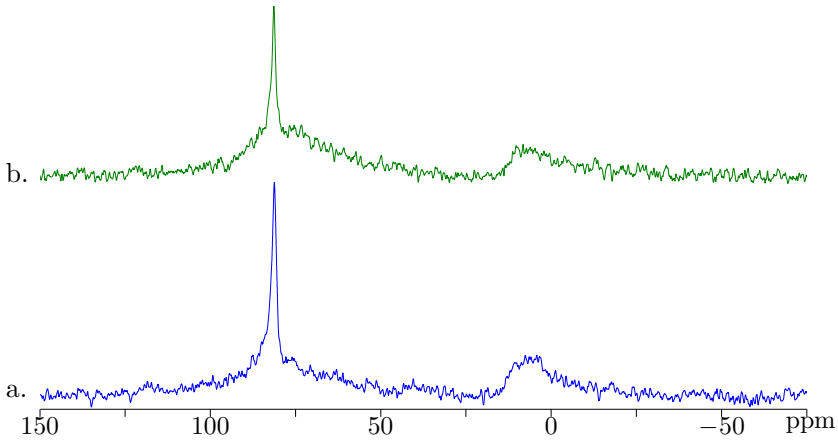

Figure 3.11: ^{27}Al NMR of ZnO with 2 atom% Al, dried at 90°C then annealed at a) 500°C and b) 600°C.

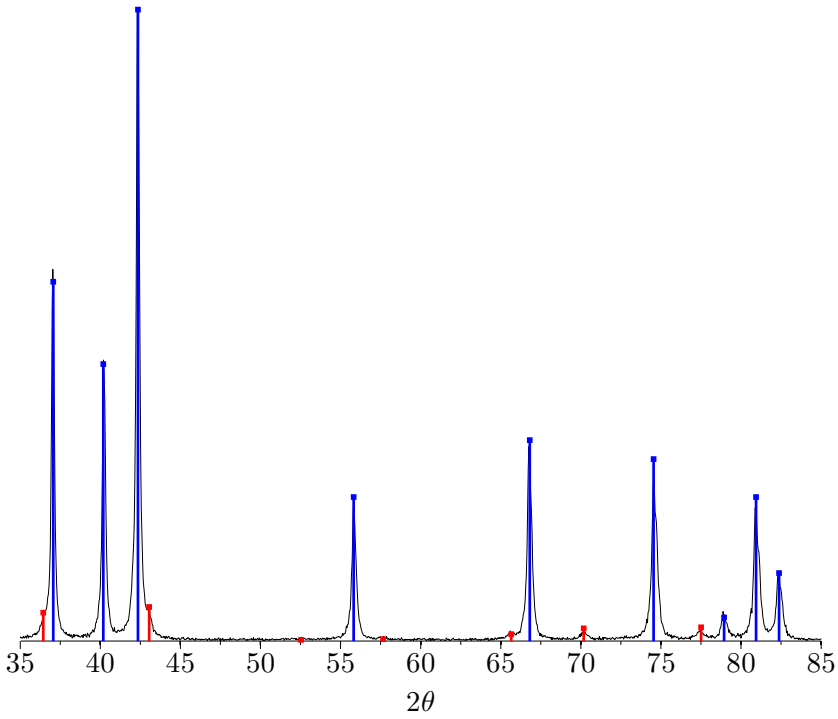

Figure 3.12: XRD trace of ZnO containing 8 atom% Al showing both the zincite (blue) and gahnite (red) phases.

viding the source of its n-type semiconductor behavior [77]. However, under these conditions the Al ions that occupy the zincite Zn sites can easily move to

a preferred interstitial position [78].The migration to interstitial sites by both Zn and Al would reduce the symmetry of the crystal resulting in broadened NMR lines. Furthermore, movement of Al ions from Zn sites to interstitial sites would reduce the intensity of the 81.2 ppm signal and increase the intensity of the 75 ppm signal. An alternative to heating under vacuum is to anneal under a reducing atomosphere e.g. H_2/N_2, to maximise oxygen vacancies.

The NMR spectra of samples heated at a range of temperatures up to 600°C for 2 hours under vacuum showed accelerated broadening of the 81.2 ppm line width compared with those heated in air for an additional hour, and there was a marked increase in the relative intensities of the 75 ppm and 8 ppm signals (Figure 3.13). Interestingly the previous thermal history of the sample had a large influence over its behavior during the vacuum annealing step. Thus samples heated with slower heating profiles, produced larger and narrower signals for the tetrahedral signal at 75 ppm, and octahedral signals at 8 ppm.

The annealing temperature under vacuum needs to be high enough to allow some Zn ions to move to interstitial positions, but if the annealing temperature is too high, the Al ions can also take up interstitial positions, which would result in a net removal of carriers [79].As a result there is a small temperature window where the presence of Al doping increases the ability to provide higher carrier concentrations. The NMR study therefore suggests that vacuum annealing should be restricted below 600°C in order to prevent the loss of carrier density due to the presence of interstitial Al.

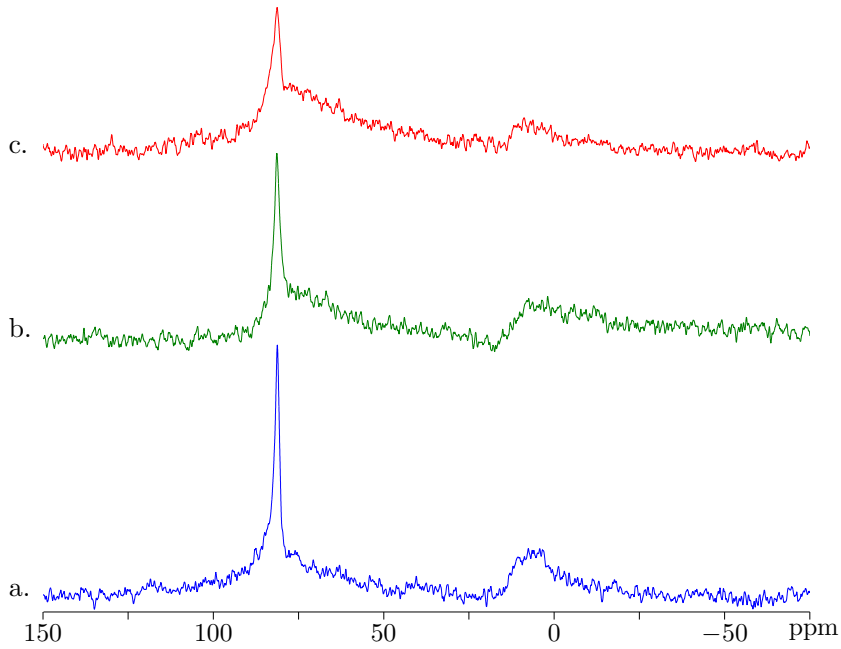

Figure 3.13: ^{27}Al NMR of ZnO with 2 atom% Al dried at 90°C then a) annealed at 500°C before being post-annealed under vacuum at b) 400°C and c) 600°C.

3.4 Variation of Dopant Level

A series of samples was prepared using EA containing 0.5, 1, 2, 4 and 8 atom% Al respectively. Samples were dried at 90°C prior to calcination at 500°C in a preheated furnace. The 4 atom% Al sample showed a marked broadening of the 82 ppm signal, compared with the 1 and 2 atom% Al doped samples, indicating that the higher Al concentration is destroying the symmetry in the zincite structure. More marked in the 8 atom% sample was the much higher intensity of the broad tetrahedral signal at 75 ppm and octahedral 8.2 ppm signal. An additional weaker broad feature centered at *ca* 45 ppm is also visible in this sample (Figure 3.14) which has been attributed to pentacoordinate Al [80].

A number of possibilities exist to explain these changes in the spectra. It is likely that some Al is migrating into the tetrahedral interstitial sites of the

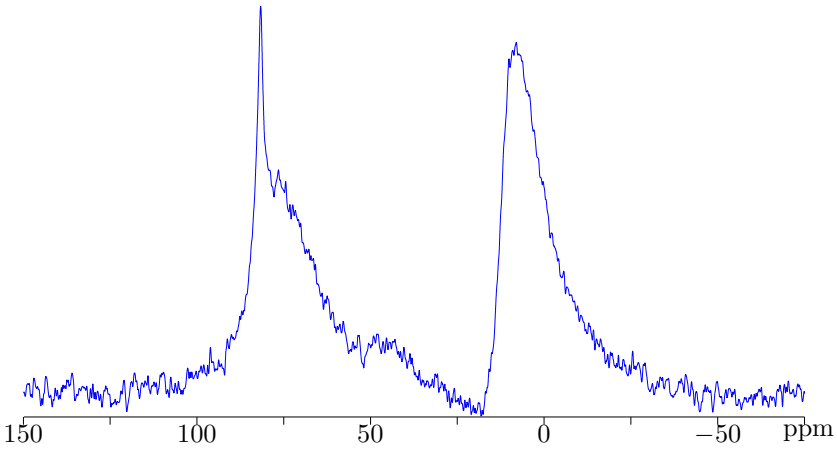

Figure 3.14: ^{27}Al NMR of ZnO with 8 atom% Al, dried at 90°C and annealed at 500°C

zincite structure. The behaviour observed on annealing under vacuum previously (see above) suggested that this could account for some proportion of the signal observed *ca* 75 ppm. A second possibility is that these signals are due (at least in part) to an amorphous phase incorporating Zn as well as Al.

To examine this possibility in more detail, a precursor containing a Zn:Al ratio of 1:2 which was consistent with the $ZnAl_2O_4$ phase was prepared. Calcination at 500°C gave a ^{27}Al NMR spectrum consisting of 3 broad peaks, centered at 7, 37.4 and 70 ppm, (Figure 3.15) approximately in proportion to the intensity of the broader peaks seen in the 8 atom% Al doped samples. This sample was amorphous to X-rays, however the gahnite phase (JCPDS card No 05-0669) commenced crystallization on calcining at 600°C (Figure 3.16) . While no other phase was observed at this temperature the lines were relatively broad and weak. Further heating at a higher temperature was necessary to produce a well crystallised material. Some tetrahedral (75 ppm) Al remained at 600°C, but above 700°C the ^{27}Al NMR spectrum showed a single sharp signal exhibiting a quadrupolar line shape centered at *ca* 10 ppm (Figure 3.17). Thus

crystallisation of the spinel structure of gahnite resulted in the Al ions exclusively adopting octahedral lattice sites.

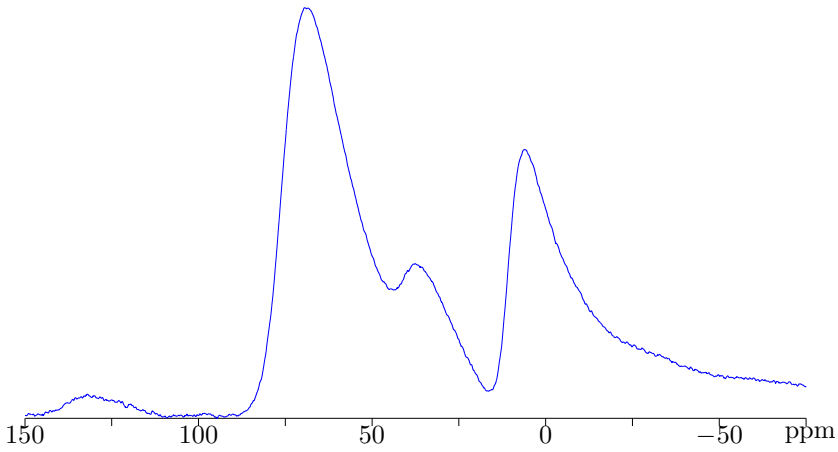

Figure 3.15: NMR of $ZnAl_2O_4$ phase annealed at 500°C

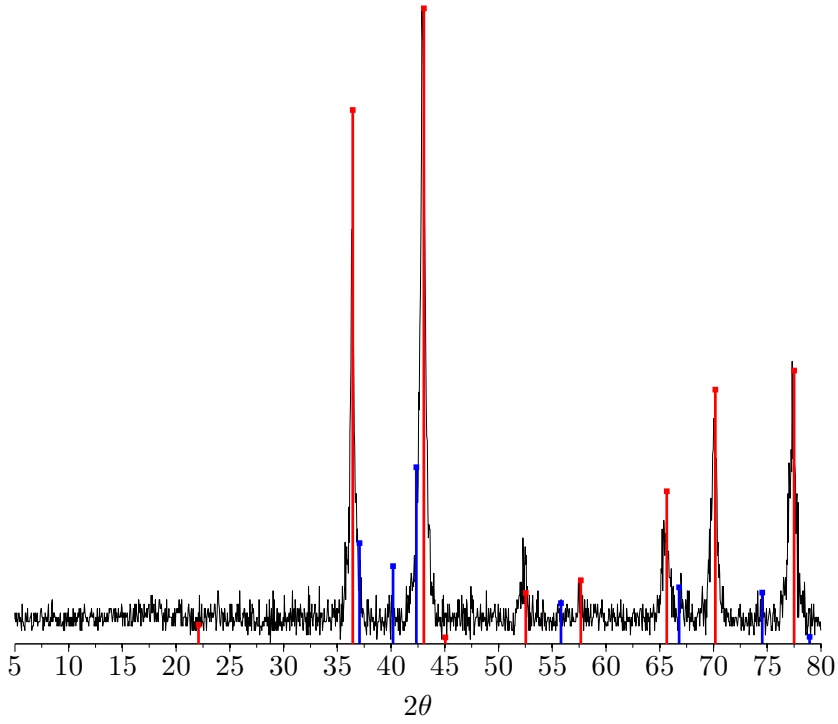

Figure 3.16: NMR of $ZnAl_2O_4$ phase annealed at 500°C

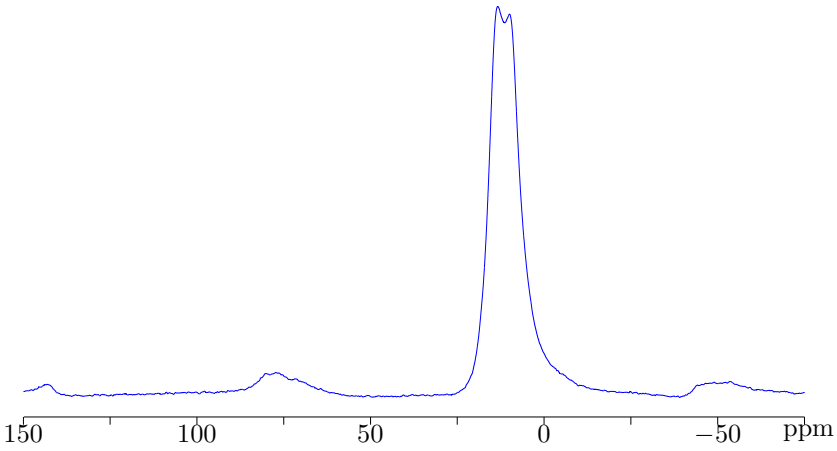

Figure 3.17: NMR of $ZnAl_2O_4$ phase annealed at 800°C

A further possibility, which is considered to be less likely, is that the broader signals in the Al-doped Zn samples are due to the tetrahedral and octahedral Al signals observed in γ-alumina during the thermal evolution of sol-gel derived alumina [81]. However, the proportion of tetrahedral aluminium in the current samples is much greater, and the peak positions are shifted slightly to lower field (5ppm, 65 ppm). No evidence for γ-alumina was observed in the powder XRD patterns.

3.5 Quantitative Powder X-ray Diffraction

XRD data were collected on a range of ZnO powders containing various Al contents. These samples were produced under conditions to maximize the level of Al substitution into the Zn lattice sites - as determined by maximization of the relative peak height of the 81.2 ppm ^{27}Al NMR signal. This method used a sol precursor containing EA, dried at 90°C followed by rapid calcination at 500°C in a preheated oven. Zincite (JCPDS library file 36-1451) was the only phase observed. Figure 3.18 shows the crystallite size variations in the series, where the increase in dopant concentration resulted in smaller crystallite sizes. It

has previously been shown that incorporation of dopant increases the density of nucleation sites [82].

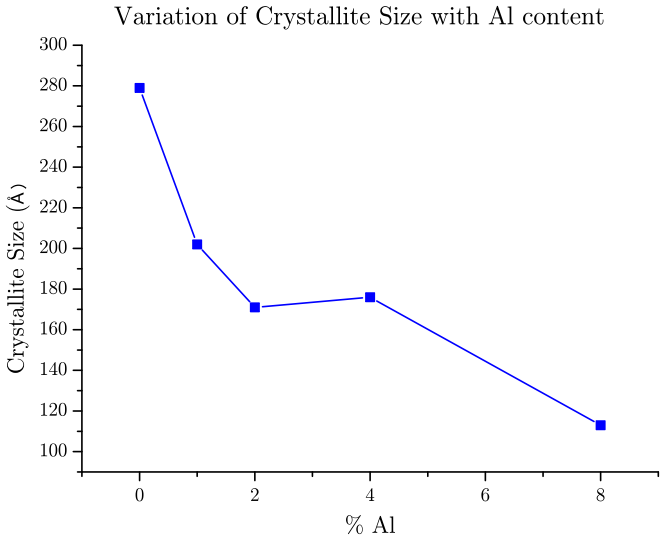

Figure 3.18: Crystallite size variations with respect to Al concentration

Accurate unit cell dimensions were calculated using TOPAS XRD software. Variation of crystallographic a and c lattice parameters were found with increasing dopant level. The variations are relatively small, with both dimensions reducing slightly as the Al content increases, as might be expected on substitution of the smaller Al^{3+} ion into Zn^{2+} ion lattice sites.

It is worth comparing the variations in synthesis methods between the results observed here and the results observed in a preliminary study [83] to explain the anomalies in the X-ray data. In the previous study [83] the samples were prepared from a precursor containing MDEA, using a 160°C dwell time followed by a slow heating (5°C min^{-1}) to 500°C. By comparison with the information discussed above in the current study, it is postulated that these previous samples contain significant interstitial Al^{3+} in addition to substituted

Al^{3+} ions in tetrahedral Zn^{2+} sites in the crystal structure. This resulted in larger variations in cell dimensions across the series and showed that increasing the Al doping levels has the effect of increasing the c-axis dimension while at the same time decreasing the a-axis length. Above 4 atom%, there is no further variation in cell dimension, indicating an apparent maximum level of Al incorporation. However, this does not imply that all of the available Al is actually incorporated into the ZnO at a given level of concentration; as the solid state NMR study implies a significant proportion of the available Al is not incorporated. Figure 3.19 shows sharp signals for the tetrahedral Al incorporated into the crystalline zincite structure at 81.2 ppm. Broader peaks suggestive of gel-like alumina appeared at 75 ppm, 45 ppm, and 8.2 ppm typical of 4, 5 and 6-coordinate Al respectively.

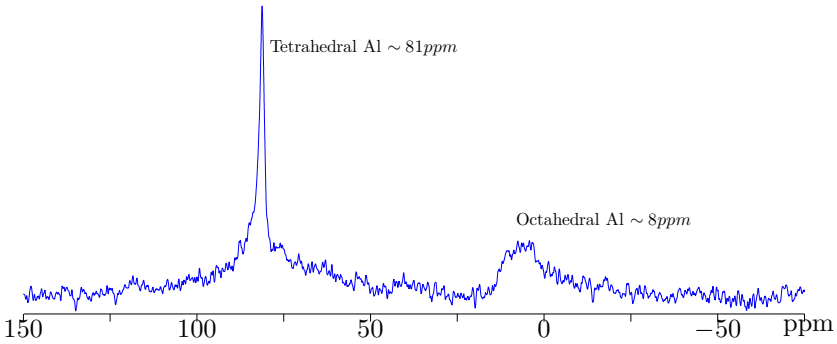

Figure 3.19: ^{27}Al NMR of ZnO with 2 atom% Al, dried at 90°C before annealing at 500°C.

The integration of solid state ^{27}Al NMR signals is not reliable in determining the relative abundance of each signal type, so it can only be estimated that in this experiment the maximum incorporation of Al into the zincite structure is somewhat less than the doping concentration. However, optimum dopant levels required to maximise conductivity have been reported at approximately the same levels [84]. Excess dopant may be problematic due to the potential

for accumulation in grain boundaries, resulting in higher resistivity.

A series of SEM micrographs are shown of ZnO samples containing 0, 1, 2 and 4 atom% Al, produced using a sol precursor containing EA, dried at 90°C followed by rapid calcination at 500°C in a preheated oven.

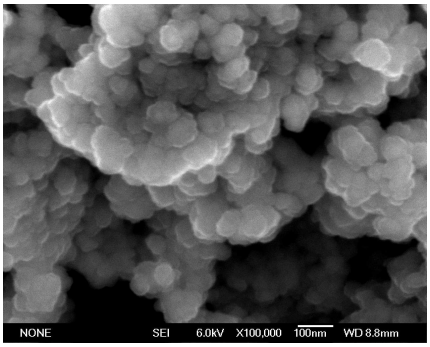

(a) 0 atom% Al

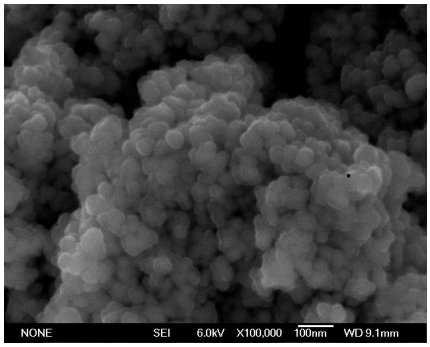

(b) 1 atom% Al

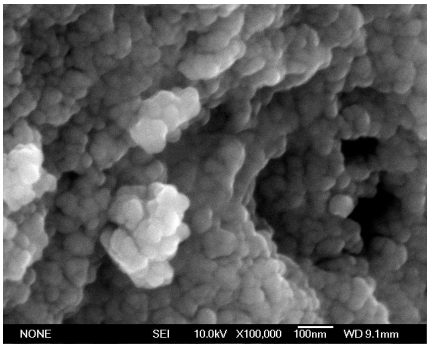

(c) 2

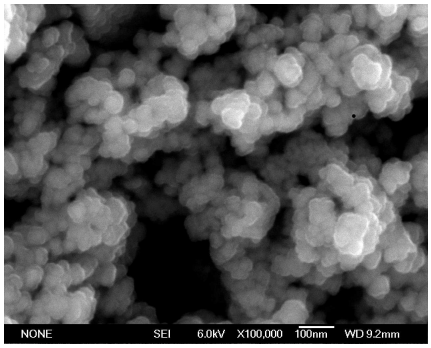

(d) 4 atom% Al

Figure 3.20: SEM micrographs of pure and Al-doped ZnO (5mm = 100nm) 100,000x magnification .

These show a reduction in crystallite size with doping level, from around 30nm for the undoped samples, to approximately 10nm for sampled containing 4 atom% Al. This is consistent with the XRD data (Figure 3.18), as well as results from high temperature (1200°C) processed ZnO [42] where the lattice parameters were both smaller for Al-doped ZnO.

3.6 Summary

The results from this study of the ZnO:Al bulk material identified several conditions under which Al incorporation and crystallite orientation can be optimised.
Of the several aminoalcohols investigated, ethanolamine (EA) was found to be most effective in terms of encouraging Al incorporation into the tetrahedral zincite sites. This is thought to be because of its lower boiling point, evaporating more quickly during annealing and facilitating the uptake of Al during crystallisation.

The concentration of dopant added is important, with the effective doping concentration being much less than that of the precursor. 0.5-1 atom% Al was found to be the best doping concentration, as with higher concentrations of Al, incorporation into the lattice sites slows, and Al is seen to segregate into the grain boundaries.

A heating profile comprised of a pre-annealing step at 90°C followed by annealing at 500°C in air gave the best result in terms of Al incorporation. Post -annealing under vacuum at 500°C served to reduce the octahedral resonance, but resulted in a broad shoulder forming on the tetrahedral peak, making its effect harder to characterise.

Quantitative XRD shows a reduction in crystallite size with increasing Al concentration.

Identifying and understanding these factors was important in order to produce thin films with desirable optical and electrical properties.

Chapter 4

Thin-Films

4.1 General

The sols from which the powders in the previous section were derived, were used to fabricate thin films. The thermal processing conditions shown to maximise Al incorporation and encourage preferential c-axis orientation in the bulk material were used, and while this did not guarantee the same results, it was thought to show similar trends. The concentrations were all 0.5M, with 2 mole equivalents of EA (with respect to Zn), and dopant Al concentrations ranged from 0-4 atom%. The only modification made was the addition of a non-ionic surfactant, Brij 97 (polyoxyethylene 10-oleoyl ether), at a concentration of 1% w/w, to aid in the wetting of the substrate.

Film thickness was of the order of 100 nm and nanocrystallites were preferentially aligned along the (002) plane (c-axis) according to XRD (refer to Figure 4.1). Interestingly, these samples showed that higher dopant levels resulted in increased c-axis alignment. Given that the levels of inter-grain alumina are also likely to be high, it is predicted that these are less likely to demonstrate low resistivities.

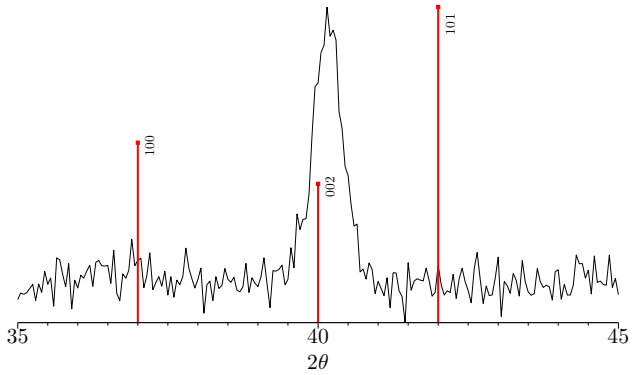

Figure 4.1: 1 layer, 2 atom% Al heated with *Hotplate* profile.

Initial films were coated onto glass substrates, as these are inexpensive, and suitable for thermal processing at the low temperatures used. The parameters for spin coating a suitable film i.e with even coverage of the substrate and without defects such as streaking or pinholes, were determined using films coated onto glass substrates. When this process was optimised, films were then coated onto quartz substrates, which were more suitable for measuring film properties such as resistivity and transparency.

4.2 Spin-coating

The substrates were cleaned by soaking overnight in a concentrated solution of mildly alkaline Pyroneg glass-wash powder in distilled water. They were then rinsed with distilled water, and dried with lint-free tissue. This also removed any residual particulates on the substrates. The surfactant was added to the sol gels, which were thoroughly mixed and allowed to settle. Before being deposited onto the substrate, the sols were filtered through a 0.2 μm syringe filter. Samples were spun at 3000 rpm for 30 seconds using a spin coater (Laurell Technologies Model WS-400E-6NPP-Lite). A sequential heating treatment

followed, with several variations investigated (based on the results from the powders) to better determine the effect of the heating profile on the properties of the resulting films. Multi layer films were achieved by repeating the spin-coating process after each heat treatment.

Effect of Ethanolamine

It was demonstrated in the previous chapter that the presence of an aminoalcohol has a marked effect on the crystallisation process and incorporation of Al into the crystal structure of ZnO:Al powders. Accordingly, the choice of aminoalcohol is thought to play a role in the crystal orientation of thin films, in terms of influencing any preferential orientation as well as the level of effective Al incorporation, both of which are factors considered when optimising the electrical and optical properties.

Structural relaxation of the film before crystallisation occurs has been identified as an important step in gaining denser films with strong preferential orientation [9]. Higher boiling point solvents and slower heating rates would assist this, as evaporation during heating would occur more slowly, allowing more time for structural relaxation, and avoiding porous films [85]. It would be expected that preferential alignment of the crystallites could occur much more easily in denser films compared with those that are more porous.

Ethanolamine has a boiling point of 170°C, and serves to coordinate Zn atoms. Because of its high boiling point, it is expected that it remains in the films both during and after crystallisation, and as such, has an effect on the molecular scale on the behaviour of the film when it crystallises [9].

4.3 Thermal Processing

It has been well documented [9, 40, 48] that the pre-heating temperature used when fabricating thin films has effects on both the physical morphology and crystalline film structure. Specifically, the grain size and density are known to increase with higher pre-annealing temperature up to a limit of around 300°C [48]. The porosity was also noted to increase with increasing pre-treatment temperature [40].

Directional heating using a hotplate was mentioned in the literature as being assistive in producing films with preferential (002) c-axis orientation, which has been associated with lower resistivities [40]. This was investigated compared with non-directional heating methods for both single and multilayer films (Figure 4.2). Films containing 2 atom%Al were heated at 90°C for 15 minutes in a pre-heated oven and on a hotplate respectively. XRD patterns of the films show the presence of only an (002) peak for both heating methods, but this is much stronger and sharper for the films subjected to directional heating, as expected.

The effect of temperature on the extent of preferential alignment aided by directional heating was also considered, with further films containing 2 atom% Al heated on a hotplate for 15 minutes at different temperatures. Characterisation with XRD showed 3 peaks, the broad (100) and (101) peaks either side of the sharper (002) peak. In the single layer films, heating at 160°C and 250°C had approximately the same effect on the crystallite orientation, while heating at 90°C showed the highest degree of preferential c-axis alignment (Figure 4.3a). Films with two layers showed an almost random orientation when heated at 250°C, while samples heated at 90°C and 160°C had sharper

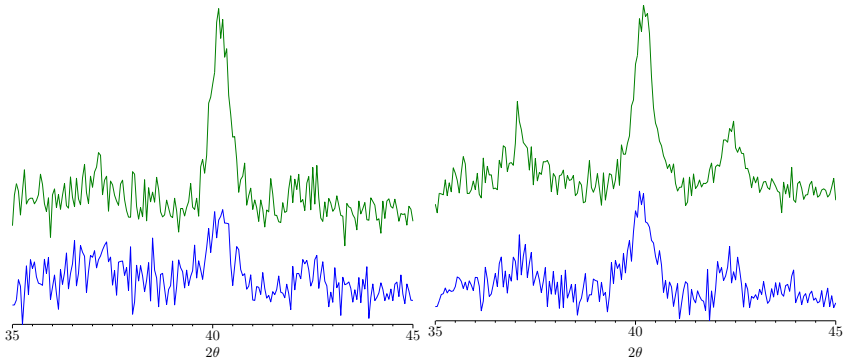

(a) 1 layer (b) 5 layers

Figure 4.2: XRD patterns comparing films pre-heated at 90°C in an oven (blue) and on a hotplate (green).

and more intense (002) peaks, but still with some (100) and (101) orientation (Figure 4.3b).

Films were also heated for 15, 30, 45 and 60 minutes respectively at 90°C on a hotplate to determine whether or not the preferential orientation of the crystallites improved with time. The 1-layer samples showed little variance, displaying an approximate 1:2:1 ratio of the (100), (002) and (101) signals respectively for each of the heating durations (Figure 4.4a). Films with 2 layers gave a similar result; with films heated for longer than 15 minutes showing the same 1:2:1 ratio of peaks. The films heated for 15 minutes however, showed strong (002) alignment, with little contribution from other orientations (Figure 4.4b).

With guidance from the analogous powders, four heating profiles were selected in order to illustrate the effect of the thermal treatment on the properties of the resulting films. The heating profiles were as follows;

- *Ramp:* Heating slowly to 500°C in an oven, at a rate of 2°C min^{-1}.

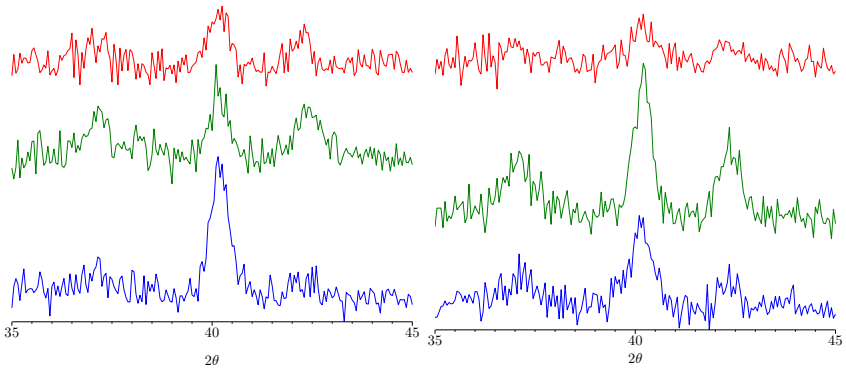

(a) 1 layer (b) 5 layers

Figure 4.3: XRD patterns comparing different hotplate pre-annealing temperatures 90°C (blue), 150°C (green) and 200°C (red)

- *Fast:* Drying at 90°C (1 hour), then annealing at 500°C (1 hour), in preheated furnaces.
- *Hotplate:* Drying on a hotplate at 90°C (15 minutes), then annealing at 500°C (1 hour) in a preheated furnace.
- *Slow:* Drying at 90°C (1 hour) with an intermediate step at 150°C (1 hour), followed by annealing at 500°C (1 hour) in a preheated furnace.

4.3.1 Post-Annealing Treatment

Many studies have been focused on the control of preferential orientation of ZnO films by their post-annealing thermal treatment [86–88]. These reports indicate that post-annealing of films in a reducing atmosphere i.e. under vacuum or a reducing gas such as N_2, decreased the resistivity of the films by a marked amount. Lee reports that electrical resistivity values of films decreased by approximately one order of magnitude after applying a second heat treatment in a reducing atmosphere [44]. In a reducing atmosphere, the number of oxygen vacancies increases, and the free carrier concentration in the film

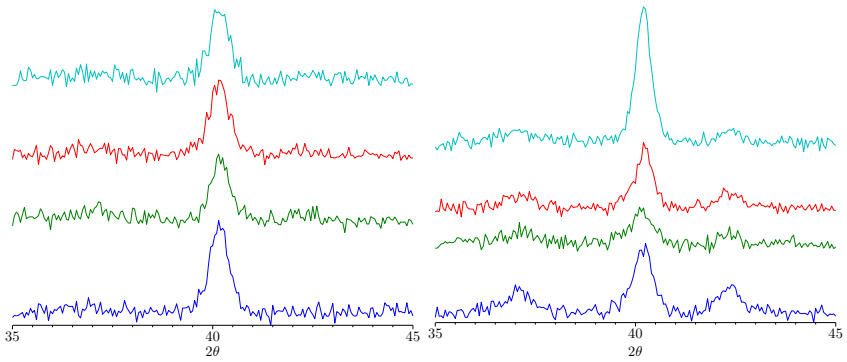

(a) 1 layer (b) 5 layers

Figure 4.4: XRD patterns comparing different durations of pre-annealing heating time on a hotplate;15 minutes (blue), 30 minutes (green), 45 minutes (red) and 1 hour (cyan).

may also be increased by oxygen annihilation from the ZnO crystals releasing carriers previously trapped in the grain boundaries [18, 55].

In following with these reports, after the initial heat treatment, films were heated under vacuum at 500°C for 1 hour, after which resistivity and transparency measurements were taken. The same films were then post-annealed again at 500°C, this time under an H_2/N_2 atmosphere for 1 hour, and the characterisation measurements repeated.

4.4 Film Structure

Ideally, films would have a very homogeneous surface so as to reduce any inelastic scattering processes occurring on the surface which can lead to increased resistivities. This type of surface morphology has been observed [23], and shows that Al-doped ZnO films are comprised of more dense grains, and

a larger number of them compared with pure ZnO films. The resulting large surface area to volume ratio makes these films suitable for gas sensing and optical applications, as it would lead to higher gas/UV adsorption and more efficient devices [59].

As seen in the powder system, the annealing temperature the films are subjected to influences the structure of the resulting films. Ohyama reports the progression from small particles arranged in a pile on top of the substrate at 300°C, to a layer of homogeneously sized particles aligned perpendicular to the substrate at 500°C, right through to random orientation of particles resulting in high surface roughness for samples heated above 600°C [9]. A decrease in this surface roughness was exhibited for one group when higher pre-annealing temperatures were used [48].

From a study of ZnO:Ga films, it was explained that the c-axis orientation can be described by Drift's "Survival of the fastest" model [89]. By this model, the initial deposition stage can produce nucleation of varying orientation, but only crystallites with the fastest growth rates, i.e. those growing away from from the substrate as opposed to growing across it and into other crystals, will survive, and in this way, preferential c-axis orientation is observed [29]. Petrov also reported that a random orientation of the crystallites is obtained during the nucleation process on non-matching substrate surface and later during film growth the crystallites are oriented with their fastest growing (001) planes, thus leading to an axial texture [90].

No other Al phase was seen in the XRD patterns of the films, suggesting that Al had been substituted for Zn in the crystal lattice, or had separated out into the grain boundaries, either way introducing little to no change in the zincite

structure [29, 59]. All films show a strong diffraction peak indication (002) orientation. The intensity of this peak, as well as of the other orientations, is shown to be affected by the annealing temperature as well as the Al concentration and film thickness.

Studies have shown a decrease in the FWHM of the (002) peak, implying more crystalline samples with increased grain size, with an increase in the pre-annealing temperature [40, 48]. It has also been demonstrated that increases in the Al concentration have the opposite effect, reducing both the grain size and crystallinity at higher concentrations [44, 59]. This may be due to the difference in size of the Zn^{2+} and Al^{3+} ions inducing stress into the crystal lattice with higher doping concentrations [44]. Increases in the Al concentration have also been seen to shift diffraction peaks to lower θ values, confirming the presence of Al^{3+} ions [59].
The intensity of the (002) peak was seen to increase with film thickness (Figure 4.5) and can be attributed to larger grain sizes and more crystalline films [29]. A decrease in the FWHM of this peak , indicating an improvement of structural properties with increasing film thickness is also seen, as reported by several groups [29, 91].

4.5 Visible Transparency

A table summarising the effects of different heat treatments, film thickness and dopant concentration is shown below (Table 4.1). The films showed transparency in the visible range, most with transmission above 80%. This region was of particular interest as it includes the active wavelengths of light that would be absorbed in a solar cell, and contribute to the conversion of photons

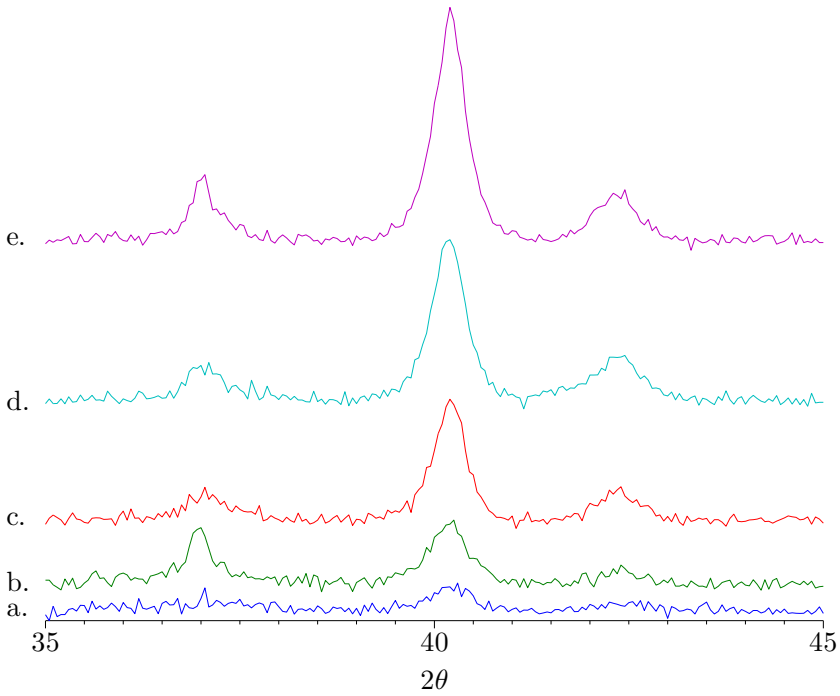

Figure 4.5: Films containing 2 atom% Al annealed using the *Hotplate* profile, with a) 1, b) 2, c) 3, d) 4, and e) 5 layers

to electrons. In this way, the average transmittance of the film, notably when used as a window layer, is a major determinant in solar cell performance [91]. Islam investigated a larger range in the spectrum, and found that more absorption occurred in thicker films at longer wavelengths, above 1000nm. This was thought to be a result of increased carrier concentrations in thicker films [91] which forecasts problems with optimising both transparency and resistivity in the same material.

All spectra showed an absorption edge at around 370nm, which corresponds with the band gap of ZnO (3.3 eV). This absorption edge was seen to shift to shorter wavelengths with increasing Al concentration, which implied an increase in the band gap because of the introduction of Al into the zincite structure [23]. This shift has been explained by way of both the Burstein-

Moss effect and the compressive strain the Al-doping induced in the film [59].

Variations in transparency were noted in relation to both the thickness of the sample, and the heating process to which the films had been subjected. For both single and 4-layer films containing 0 (Figure 4.6) and 0.5 atom% Al (Figure 4.7), heating following the *Hotplate* profile obtained the highest transparencies . Films containing 1 atom% Al, showed the highest transparencies when heated following the *Slow* profile (Figure 4.8), while films with 2 atom% Al had the best transparencies when heated with the *Ramp* profile (Figure 4.9).

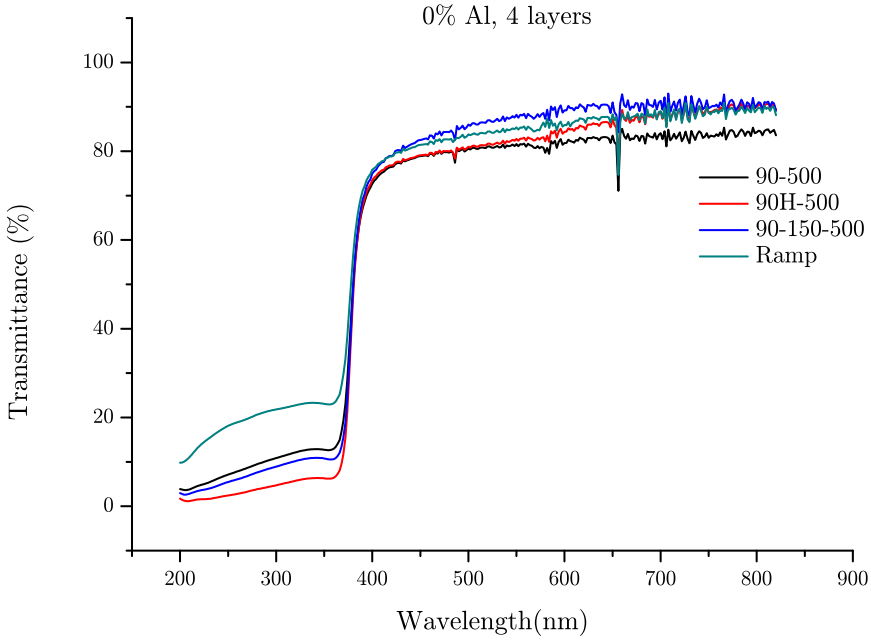

Figure 4.6: Four layer film with 0 atom% Al

From these results, it was determined that the higher the Al concentration of the film, the slower it needs to be heated in order to obtain optimum transparency. This may be due to the impact of structural relaxation of the film,

		Average Transmittance (%)	
Heating Profile	atom %Al	1 layer	4 layers
Slow	0	91	85
Slow	0.5	96	85
Slow	1	84	93
Slow	2	92	92
Hotplate	0	96	85
Hotplate	0.5	97	93
Hotplate	1	94	82
Hotplate	2	96	75
Fast	0	91	82
Fast	0.5	96	87
Fast	1	74	91
Fast	2	91	94
Ramp	0	82	86
Ramp	0.5	90	84
Ramp	1	90	87
Ramp	2	95	94

Table 4.1: Transmittance data for films over a range of Al concentrations and thermal treatments

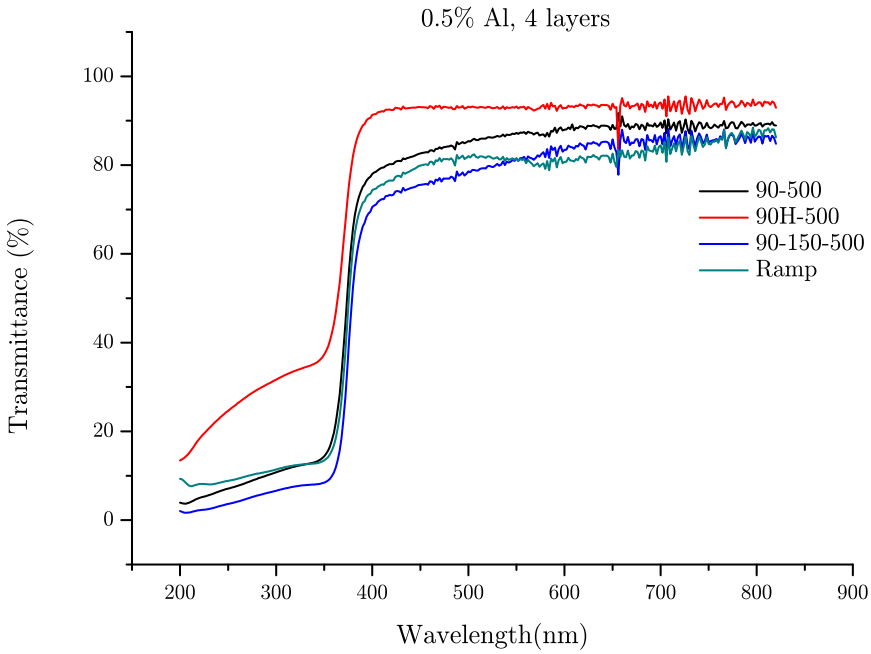

Figure 4.7: Four layer film with 0.5 atom% Al

leading to more ordered crystal orientation, as mentioned previously. The *Slow* profile which contained an intermediate 150°C step as well as the *Ramp* profile would facilitate this, with more aligned crystallites in the film serving to increase the transmittance.

The effect of the rate of heating, rather than the temperature of heating on the optical transmittance of the films was investigated. This was due to data obtained from the powders system, which showed that optimal incorporation of Al occurred for samples annealed at 500°C. An increase in transmittance with higher temperature treatments had been observed [48], and may be because of less optical scattering from denser grains, as well as grain growth reducing the amount of material in the grain boundaries [48].

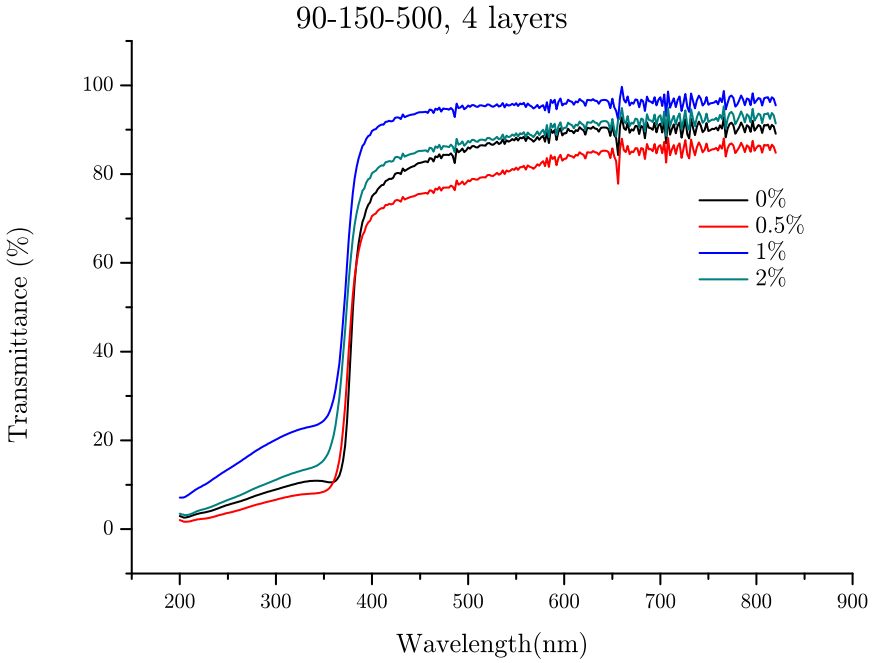

Figure 4.8: Four layer films with 1 atom% Al heated with *slow* profile.

It was found that undoped and 0.5 atom% Al doped films showed much higher transmittance in the single layer films compared with the 4-layer films, while higher Al concentrations show little difference between the thicker and thinner films. This may be because of the relatively small difference in thickness between these two sets of films. In general, thinner films are shown to exhibit higher transmittances on average than thicker films, a trend which has been commonly observed [29, 52, 91, 92]. This has been attributed to increased emissions from defects in the films, the intensities of which have been found to increase with film thickness [92].

Interestingly, the films heated using the *Ramp* profile clearly showed higher transmittance with higher amounts of Al. This trend follows with the results of Periasamy [59] who observed transmittances over 85% with a doping concen-

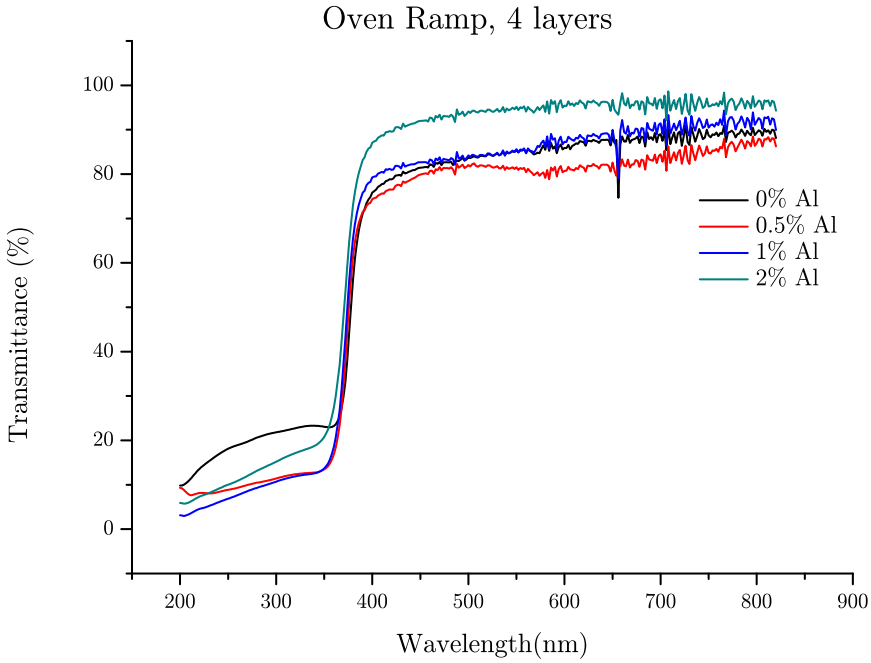

Figure 4.9: Four layer films with 2 atom% Al heated with *Ramp* profile.

tration of 6 atom% Al. In contrast, Lee reported higher transmittances for 1 atom% Al doped films, compared with lower values for the undoped, and more highly doped films containing 2 and 3 atom% Al [44]. Other heating profiles studied failed to exhibit any clear trends with regards to Al concentration.

4.6 Resistivity

Resistivity measurements were carried out on a sample of 32 films, each with a different combination of Al content, thickness and heating profile. Films with 1 and 4 layers were characterised to determine any differences in electrical and optical properties caused by the amount of material in the film. The electrical conductivity of the films is dependant on the free carrier concentration within the material, and thus can be affected by all of these variables.

These films were all treated post-annealing by heating at 500°C for an hour under vacuum after their initial heat treatment. Attempts to make resistivity measurements on films which had not been subjected to treatment in a reducing atmosphere resulted in high resistivities.

The general trend with all films was a reduction of resistivity with an increase in Al doping concentration up to 1 atom% Al, after which the resistivity began to climb. This has been well explored [58,59,93] and is a result of the addition of Al providing more free carriers in the material, up to a point where the addition of more Al leads to segregation of Al in the grain boundaries with higher doping concentration, which serves to increase the resistivity of the films.

Of the single layer films, those with 0.5 and 1atom% Al and subjected to directional heating, following the *Hotplate* profile, showed the lowest resistivities (Figure 4.10). The four layer films also gave the best result when doped with 0.5 and 1 atom% Al, but in contrast, when heated following the *Fast* profile (Figure 4.11). These observations can be explained by the structural properties of the films, in terms of crystallite size and orientation. It has been established that resistivities are lower when the film is more crystalline and highly (002) oriented [11,18].

In general, the 4-layer films showed lower resistivities compared with their 1 layer equivalents. This behaviour is well documented [23,29,46]. It can be attributed to the increase in carrier concentration with increasing thickness, due to increasing grain size incorporating previously 'trapped' material from the grain boundaries and thus reducing their negative contributions [18]. Thinner films are likely to have more surface defects such as pinholes, as a result of incomplete atomic bonding, which can act as carrier traps, in a similar way to

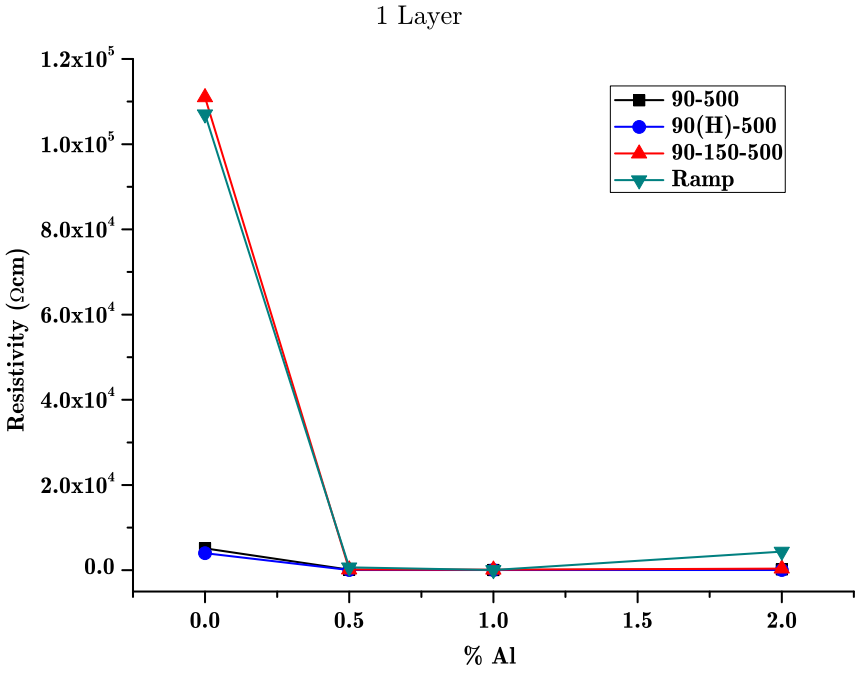

Figure 4.10: Resistivity, 1 layer, diff heating.

grain boundaries. These immobilise a proportion of the carriers, and so take on an electrical charge, which reduces mobility further by acting as a potential barrier in the film [91]. Previous work has noted the complex effect of film thickness on resistivity values [92], with wide variance in the resistivities of pure ZnO films observed with increasing thickness [23].

Of the 4-layer films, the lowest resistivities were demonstrated by films heated non-directionally, which implies a lesser degree of preferential c-axis orientation, while the highest resistivities were found for films heated on a hotplate, as shown below. This may be a result of the influence structural relaxation of the film has over the crystallisation process. Films heated slowly have more time to crystallise, and solvents can evaporate less rapidly, and thus have less effect on the composition and molecular structure of the final film [23]. Higher

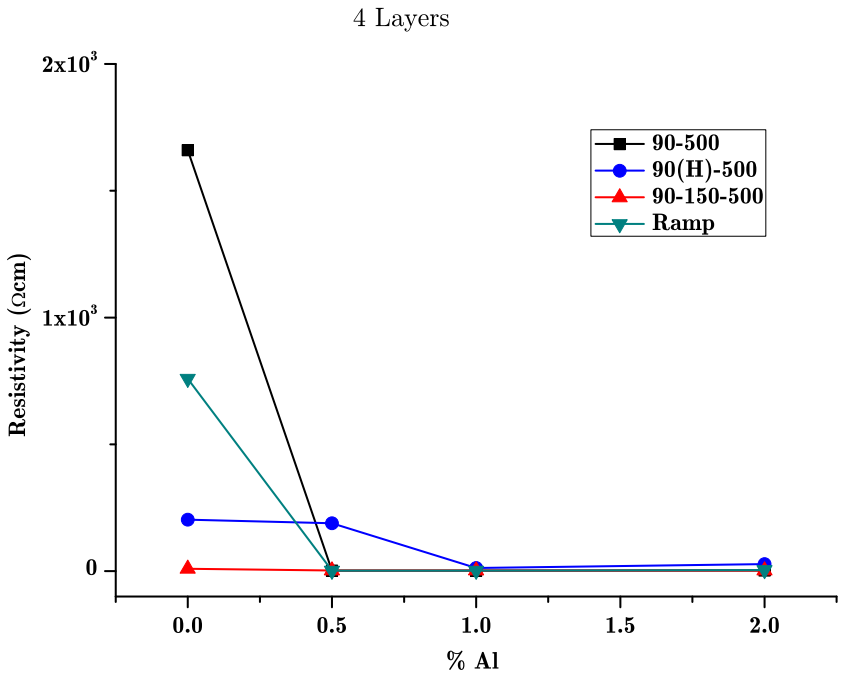

Figure 4.11: Resistivity, 4 layers, diff heating

crystallite orientation has been shown to be effective in reducing the resistivity of ZnO:Al thin films [58].

Effect of Post-annealing under H_2/N_2

Post-annealing treatment under a reducing atmosphere of H_2/N_2 proved to reduce the resistivity of the films by around an order of magnitude, as has been seen in other work [44].This was best exemplified for films heated with the *Hotplate* profile, as shown below (Figure 4.12);

4.7 Summary

For films post annealed under vacuum, the lowest resistivity was shown by a film containing 1 atom% Al, heated using the *Fast* profile. The highest was

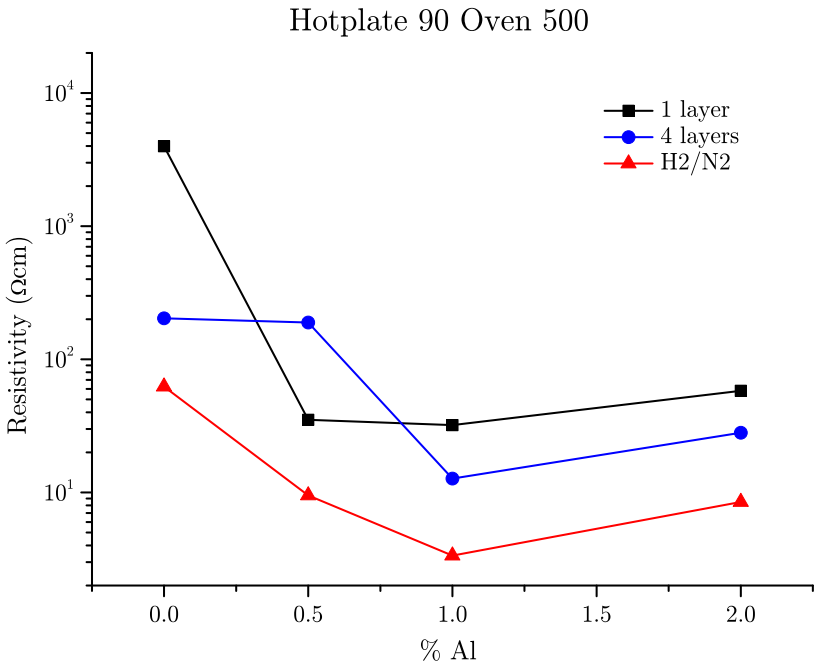

Figure 4.12: Resistivity as a function of Al content for samples heated on a hotplate.

seen for a sample with 1 atom %Al, heated with the *Hotplate* profile.

When films were subjected to further post-annealing under H_2N_2, the resistivities dropped by around an order of magnitude, with the lowest resistivity shown for a sample containing 1 atom%Al, heated using the *Slow* profile, while the highest was shown with 0.5 atom%Al heated with the *Hotplate* profile.

Transparencies for all films were above 80% in the visible range, and thicker films generally demonstrated lower transmittances. Films with higher Al concentrations gave higher transmittances when heated using slower profiles, which allowed more time for structural relaxation and incorporation of dopant into the film. Films with lower Al concentrations gave higher transmittances

		Resistivity (Ωcm)	
Heating Profile	Al (atom%)	Vacuum	H_2N_2
Fast	0.5	$1.97x10^{0}$	$2.02x10^{0}$
Ramp	0.5	$2.23x10^{0}$	—
Slow	0.5	$2.56x10^{0}$	$5.84x10^{0}$
Hotplate	0.5	$1.89x10^{2}$	$9.50x10^{0}$
Fast	1	$1.83x10^{0}$	$1.69x10^{0}$
Ramp	1	$2.06x10^{0}$	—
Slow	1	$2.47x10^{0}$	$8.98x10^{-1}$
Hotplate	1	$1.27x10^{1}$	$3.36x10^{0}$

Table 4.2: Resistivity data for films over a range of Al concentrations and thermal treatments

when heated following the *Hotplate* profile, which implies preferential c-axis orientation of the crystallites is important for films with 0.5-1 atom% dopant.

Increased film thickness gave films with lower resistivities, but also lower transparencies. This results in a trade-off between optical and electrical properties in terms of film thickness.

The most successful films produced, exhibiting the best balance of desirable characteristics such as low resistivity and high transparency contained 0.5 atom% Al and were heated following the *Fast* profile, which comprised pre-annealing at 90°C for an hour before annealing at 500°C, followed by vacuum and H_2/N_2 post-annealing treatments.

Chapter 5

Synchrotron Experiments

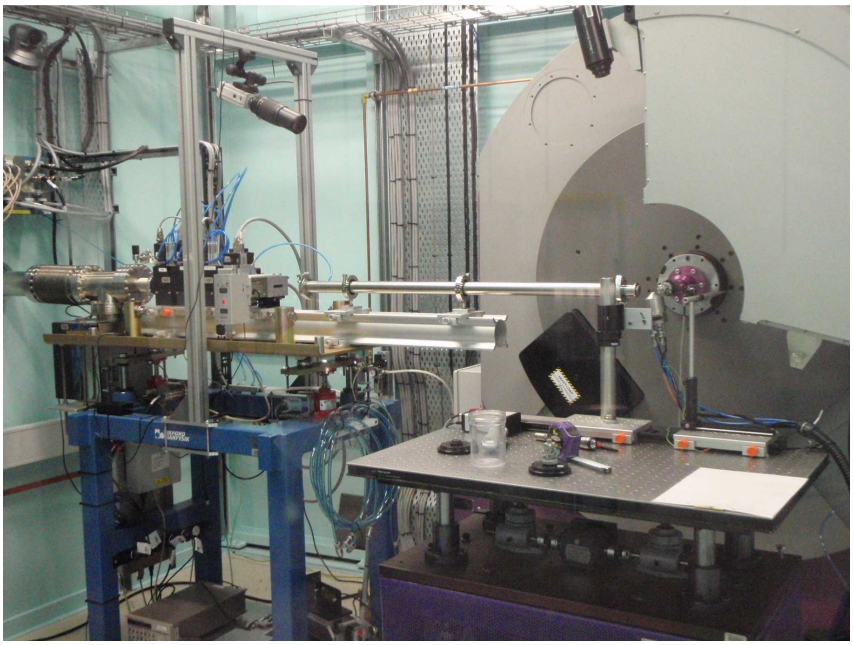

Figure 5.1: Setup of the powder diffraction beamline at The Australian Synchrotron

The kinetics of nucleation of crystalline ZnO, and dopant incorporation of Al into the zincite structure were investigated using X-ray diffraction in an attempt to provide insight into the dynamics of the crystallisation and coalescence effects in Al-doped ZnO gels. As a prelude to studies on thin films,

detailed crystallographic analysis of the materials formed from gels as a function of the deposition conditions and dopant species were carried out, with the aim of capturing the nucleation process, (in particular, the point at which the dopant begins to be incorporated into the growing crystallite) as a function of thermal treatments, dopant concentration, etc. There is no reason to suggest that the nucleation effects observed here will be any different to what occurs in a thin film.

These experiments were conducted on the powder diffraction beam line at the Australian Synchrotron, using the Cyberstar hot air blower with the Mythen detector. Gel samples in quartz capillaries were mounted in the standard fashion Figure 5.2b. Using this setup data was obtained in real-time during annealing at temperatures up to 800°C.

The synchrotron XRD experiments complement ongoing NMR and electrical measurements to give a more complete picture of the ZnO:Al system and how the processing conditions affect the structure and hence the electrical and optical properties of Al-doped ZnO thin films.

The experiments fall into two series: in situ calcination studies of pre-dried gels, and thermal treatment of pre-calcined materials. For the calcination studies, 5 different doping levels (0, 1, 2, 4, 8 atom% Al) were investigated under each condition, and a range of heating experiments were performed.

Pre-calcined samples with doping levels of 0, 1, 2 and 4 atom% Al were investigated, and were mounted in quartz capillaries sealed under vacuum. The thermal history of the samples covered a range of different heating conditions, and included samples treated pre-annealing by slow or rapid heating, followed

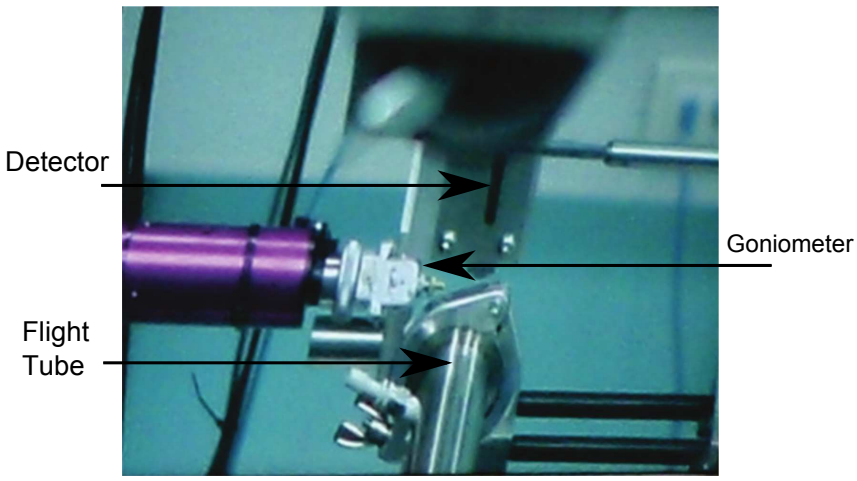

(a) Sample Mount Setup

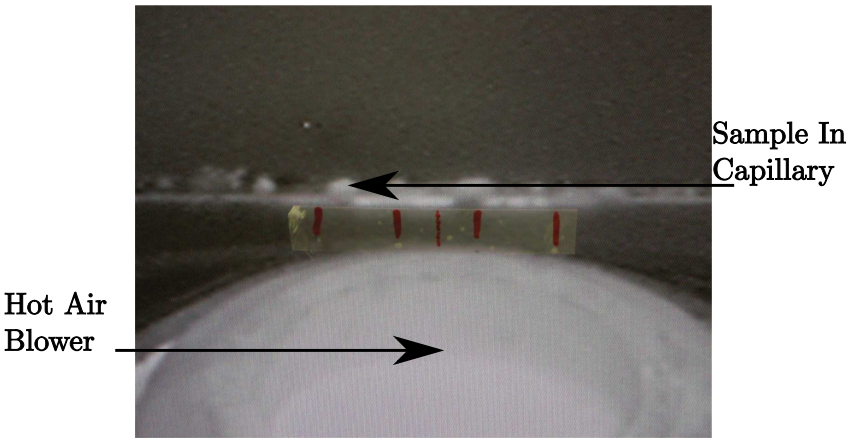

(b) Sample Mount Setup (close)

Figure 5.2: Setup of the Powder Diffraction Beamline

by rapid heating to anneal at 500 or 600°C for 2 hrs.

Synchrotron radiation was essential for these experiments because the changes of interest in the ZnO lattice parameters were very subtle, as the doping levels of Al are very low (1-2 atom%). It also facilitated in situ measurements as a function of temperature so as to observe the formation of ZnO nuclei, which are small and weakly scattering. The speed of collection was also much more efficient, with analyses made in the lab taking 4 hours compared with just a few minutes at the synchrotron.

At the time of publication, only limited data, mainly on the ex-situ series had been processed, but this gives a clearer picture of the effect of both dopant concentration and thermal treatment on these materials than had previously been obtained using lab techniques. Also shown is a time series observation of the nucleation of a sample of undoped ZnO at different temperatures (Figure 5.3).

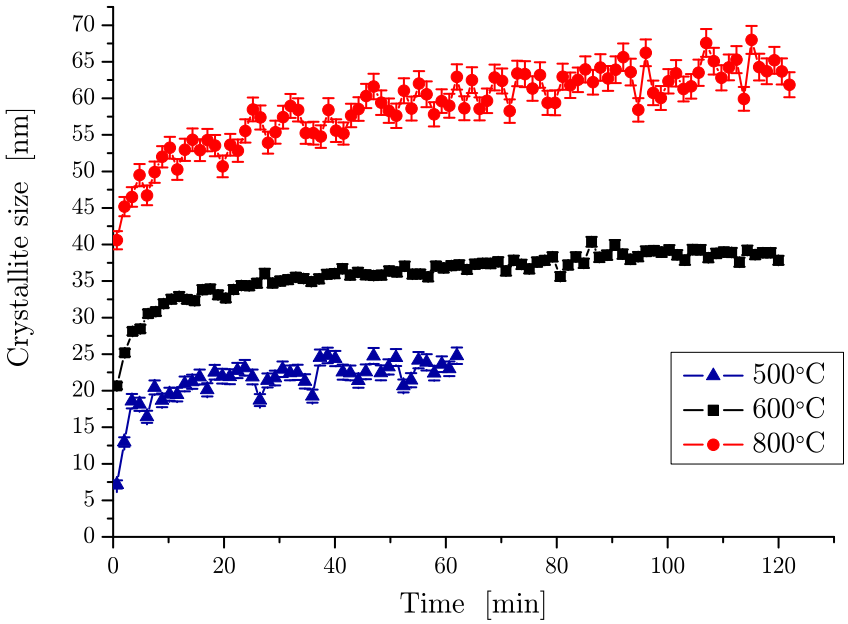

Figure 5.3: The nucleation of undoped ZnO over time at 500°C, 600°C and 800°C.

Full pattern fitting was carried out for all samples using TOPAS software. Samples annealed at 500°C, with range of Al concentrations are shown below (Figure 5.4). These show a slight increase in the FWHM of the (002) peak with increasing Al concentration, demonstrating decreased crystallinity in the material and smaller grain sizes (Figure 5.5) This agrees with XRD data ob-

tained in the lab, but provides more accuracy and reliability.

The effect of annealing temperature on these materials was also investigated, with samples annealed between 5-800°C . Results show a steady increase in crystallite size with increasing annealing temperature (Figure 5.6).

The lattice parameters for the a- and c- axes were calculated with respect to changes in the Al concentration (Figure 5.7) and annealing temperature (Figure 5.8). As shown by the error bars on the plots, there is little significant change in the lattice parameters both as a function of Al concentration and annealing temperature.

These synchrotron experiments allowed a more detailed investigation into the nucleation of Al-doped ZnO, and coupled with other results, give a greater understanding of this system, in particular the effect of different variables with regards to structure and physical properties.

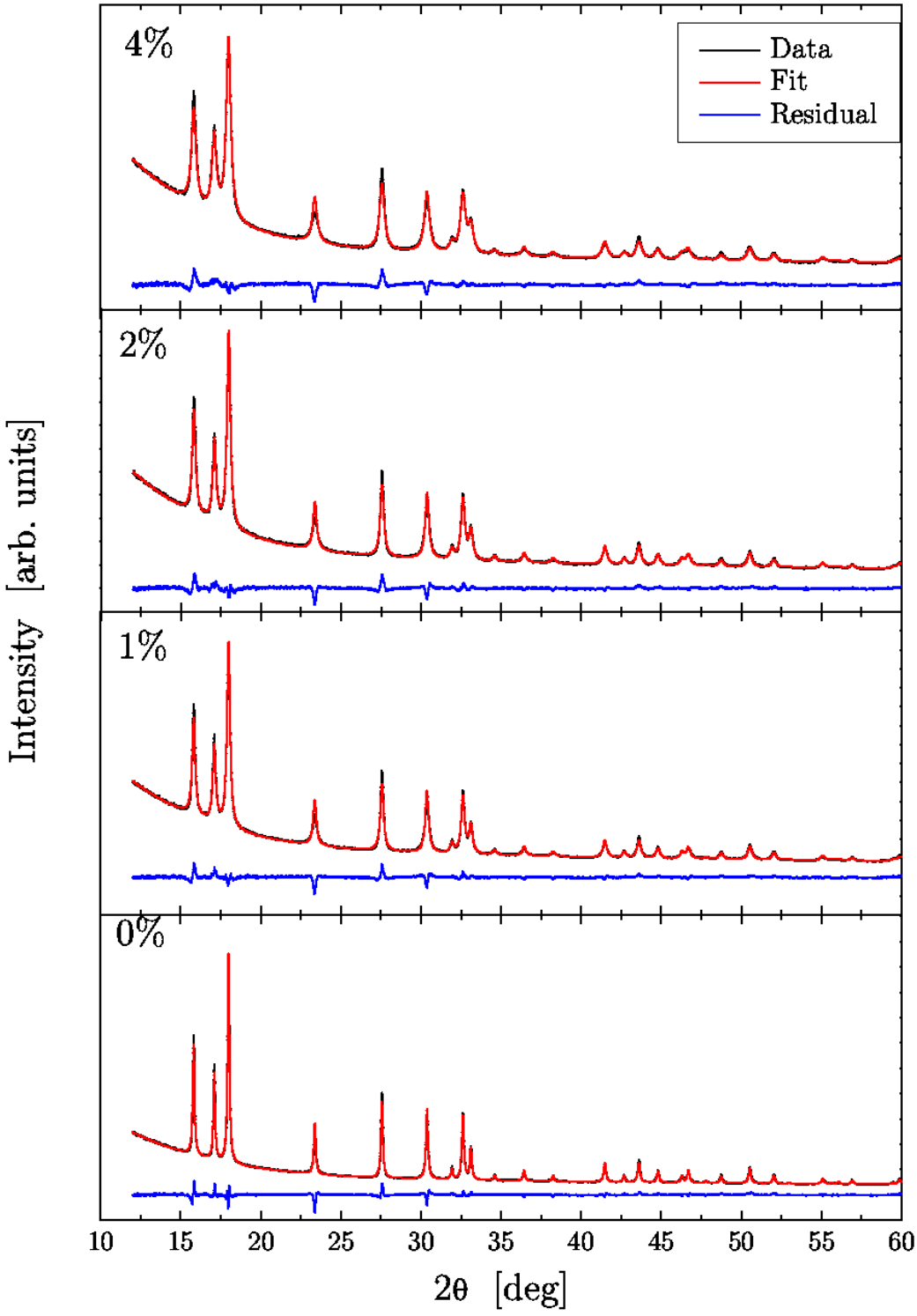

Figure 5.4: XRD patterns of ZnO with various amounts of Al-dopant

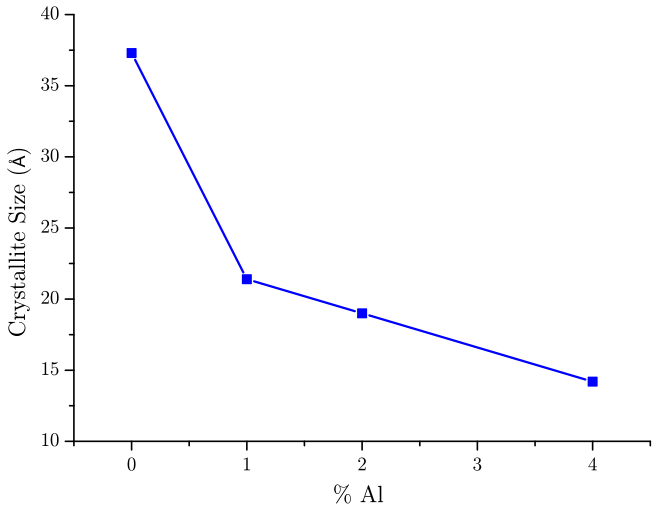

Figure 5.5: Effect of Al doping on Crystallite Size

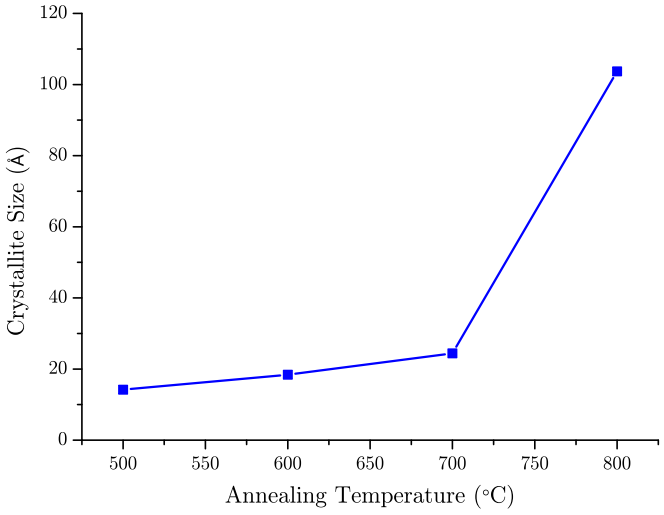

Figure 5.6: Effect of annealing temperature on crystallite size.

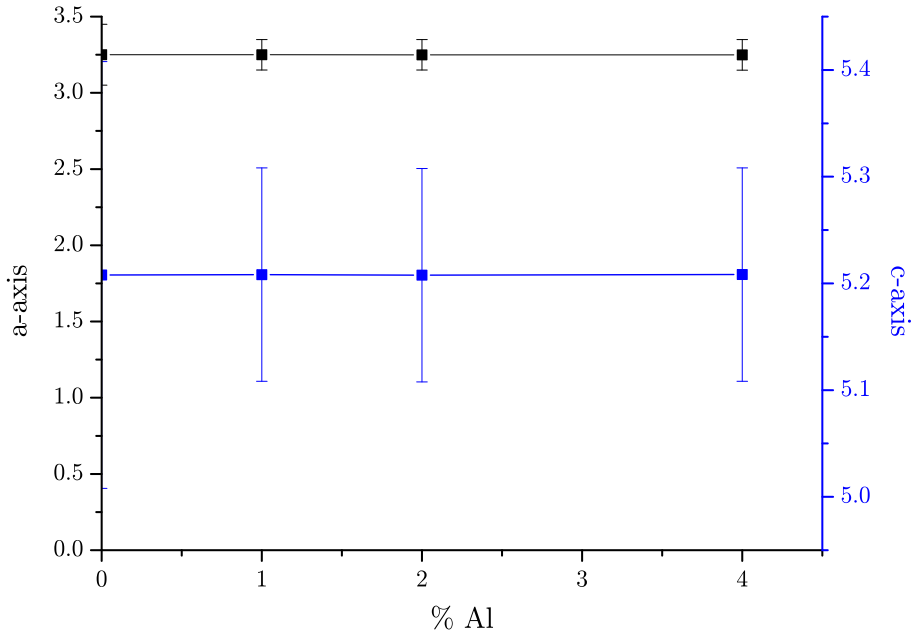

Figure 5.7: Effect of Al concentration on the lattice parameters.

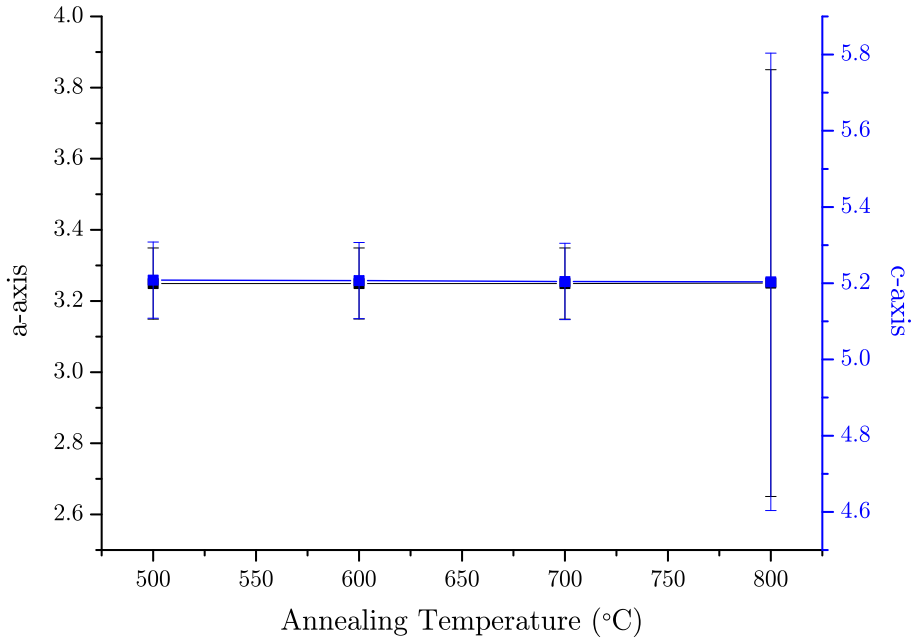

Figure 5.8: Effect of annealing temperature on the lattice parameters

Chapter 6

Conclusions

The research undertaken over the course of this thesis was an investigation into optimising the structural, optical and electrical properties of aluminium-doped zinc oxide thin films prepared via a sol-gel route, for use as a transparent conductive material. Possible applications include incorporation in thin film solar cells, flat panel displays and in gas-sensing devices.

The first section (Chapter 3) focused on a ^{27}Al NMR study of the bulk material, to understand the way in which Al is incorporated into the zincite structure. Two main environments were identified as incorporation sites for the Al - either substituting for Zn in the Zn lattice sites, or incorporating in interstitial sites. The NMR signals for these environments were seen at $\sim$ 81 ppm (tetrahedral Al) and $\sim$ 8 ppm (octahedral Al) respectively. By substituting for a Zn^{2+} ion, Al^{3+} incorporation results in a free electron, increasing the conductivity of the sample, so optimisation was directed at increasing the proportion of this type of coordination.

In samples with higher dopant concentration, broad, weak signals were also observed at 75 ppm, 45 ppm, and 8.2 ppm, which are typical of 4, 5 and 6-

coordinate Al respectively. It has been established that the effective doping concentration is in fact much less than the dopant concentration in the precursor. This has been attributed to agglomeration of excess Al in the grain boundaries, which has a negative effect on electrical properties of the material.

The incorporation of an aminoalcohol species in the precursor solution served to solubilise the ZnO:citrate complex, and also contributed to the way in which Al was incorporated into the structure. Ethanolamine, diethanolamine, methyl-diethanolamine, 2-amino-ethoxy ethanol and 1-amino-3-propanol were investigated. Lower boiling point aminoalcohols gave better result in terms of maximising tetrahedral Al coordination and minimising contributions from other coordinations. This is thought to be a result of the aminoalcohol evaporating more quickly on heating and/or remaining in the gel during crystallisation, serving to include more Al in the crystallised product, and to minimise stresses in the film during crystallisation. For these reasons, ethanolamine (EA) was chosen to be used in all further syntheses.

The thermal treatment of the bulk material was also shown to effect the incorporation of Al. The optimum annealing temperature was found to be 500°C, with a pre-annealing drying step at 90°C. Both steps involved heating preheated furnaces in air for an hour. Slower heating profiles such as heating at 5°C/min up to 500°C gave NMR spectra showing much lower signal for tetrahedral Al, and higher signal for octahedral and amorphous Al. Faster profiles such as annealing at 500°C with no drying step also resulted in lower signal for tetrahedral Al. These results show that a balance must be obtained in terms of heating speed - too slow or too fast and less of the dopant will be incorporated into a tetrahedral environment which is optimal for good electronic properties.

Post annealing treatment of the material under vacuum was effective in reducing the octahedral signal, but this was not translated to an increase in the tetrahedral signal, implying the migration of Al into higher coordination states, or out of the crystal lattice completely.

Varying the concentration of dopant between 1–8 atom% showed good incorporation up to 2 atom%, but with higher concentrations, a larger proportion of dopant was excluded, incorporated instead into the grain boundaries. Quantitative powder XRD showed a decrease in crystallite size with increasing dopant concentration.

The second section (Chapter 4) made use of the optimised processing parameters for Al incorporation, as determined for the bulk material, and applied these to the fabrication of thin films. The main focus was to create films with optimised electrical and optical properties, specifically low resistivity and high transparency. Films with 0.5-1atom %Al and multiple layers showed the lowest resistivities. All films were subjected to post annealing under vacuum at 500°C. Without this step, resistivities were high and measurements gave unreliable results in terms of the Hall effect. Further post annealing under H_2/N_2 at 500°C decreased resistivity by an order of magnitude.

Transparencies for all films were above 80% in the visible range, and the thicker multi-layer films generally demonstrated lower transmittances. Films with higher Al concentrations gave higher transmittances when heated more slowly, while films with lower Al concentrations gave higher transmittances when subjected to rapid directional heating. Preferential c-axis orientation was observed for all films, but was increased with increasing film thickness, and for films subjected to directional heating on a hotplate. Increased film thickness gave films

with lower resistivities, but also lower transparencies. This results in a trade-off between optical and electrical properties in terms of film thickness.The best films, as with the bulk material, were dried at 90°C before annealing at 500°C. This was followed by post annealing treatments under vacuum and H_2/N_2.

6.1 Future Work

To further the understanding of the processing conditions required to produce optimised thin films of Al-doped ZnO, further research should be carried out in the following areas;

- Greater insight into the nucleation process of ZnO will provide more information on optimising the incorporation of Al into these materials. This may be possible using synchrotron radiation and carrying out in situ experiments to observe and characterise the nucleation process as a function of time. This could be applied to both bulk materials and/or films.

- While it is known that thermal treatment under a reducing atmosphere maximises oxygen vacancies in the material, further investigation should be carried out as to the end position of dopant ions as a result of this treatment, by means of ^{27}Al NMR.

- Adjustments to the sol-gel solution should be looked into for creating thicker films in fewer layers. Based on the current results, this would reduce resistivities and may lessen the drop in transparency seen for films with multiple layers.

References

[1] C. Jagadish and S.J. Pearton. *Zinc oxide bulk, thin films and nanostructures: processing, properties and applications*. Elsevier, Amsterdam, 2006.

[2] K. Ellmer, A. Klein, and B. Rech. *Transparent conductive zinc oxide: basics and applications in thin film solar cells*. Springer series in materials science. Springer, Berlin, 2008.

[3] C. Liu A. Teke M. A. Reshchikov S. Doan V. Avrutin S.-J. Cho U. Ozgur, Ya. I. Alivov and H. Morkoc. A comprehensive review of ZnO materials and devices. *Journal of Applied Physics*, 98(4):1–103, 2005.

[4] T. Minami. New n-type transparent conducting oxides. *MRS Bulletin*, 25(8):38–44, 2000.

[5] M. Gabas, N.T. Barrett, J.R. Ramos-Barrado, S. Gota, T.C. Rojas, and M.C. Lopez-Escalante. Chemical and electronic interface structure of spray pyrolysis deposited undoped and Al-doped ZnO thin films on a commercial Cz-Si solar cell substrate. *Solar Energy Materials and Solar Cells*, 93(8):1356 – 1365, 2009.

[6] F. Paraguay, D., M. Miki-Yoshida, J. Morales, J. Solis, and W. Estrada L. Influence of Al, In, Cu, Fe and Sn dopants on the response of thin film ZnO gas sensor to ethanol vapour. *Thin Solid Films*, 373(1-2):137 – 140, 2000.

[7] Jeon H. Nurmikko A.V. Xie W. Grillo D.C. Kobayashi M. Gunshor R.L. Hagerott, M. Indium tin oxide as transparent electrode material for ZnSe-based blue quantum well light emitters. *Applied Physics Letters*, 60(23):2825–2827, 1992.

[8] H. Hartnagel. *Semiconducting transparent thin films*. Institute of Physics Pub., University of Michigan, 1995.

[9] Kozuka H.A Yoko T.A Sakka S.A Ohyama, M.B. Preparation of ZnO films with preferential orientation by sol-gel method. *Nippon Seramikkusu Kyokai Gakujutsu Ronbunshi/Journal of the Ceramic Society of Japan*, 104(4):296–300, 1996.

[10] A.C. Tolcin. United States Geological Survey, 2009.

[11] Dinghua Bao, Haoshuang Gu, and Anxiang Kuang. Sol-gel-derived c-axis oriented ZnO thin films. *Thin Solid Films*, 312(1-2):37 – 39, 1998.

[12] White S.P. Hendy S.C. MacKay, J.R. Modelling the growth of zinc oxide nanostructures. *ANZIAM Journal*, 50(3):395–406, 2009.

[13] Illy B.N. Mackay J.R. White S.P. Hendy S.C. Ryan M.P. Ingham, B. In situ synchrotron X-Ray absorption experiments and modelling of the growth rates of electrochemically deposited ZnO nanostructures. *Materials Research Society Symposium Proceedings*, 1017:99–104, 2007.

[14] Illy B. N. Ryan, M. P. and B. Ingham. Effect of Supersaturation on the Growth of Zinc Oxide Nanostructured Films by Electrochemical Deposition. *Crystal Growth & Design*, 10(3):1189–1193, 2010.

[15] Illy B.N. Ryan M.P. Ingham, B. Direct observation of distinct nucleation and growth processes in electrochemically deposited ZnO nanostructures using in situ XANES. *Journal of Physical Chemistry C*, 112(8):2820–2824, 2008.

[16] Illy B.N. Ryan M.P. Ingham, B. In situ synchrotron studies of ZnO nanostructures during electrochemical deposition. *Current Applied Physics*, 8(3-4):455–458, 2008.

[17] Illy B.N. Toney M.F. Howdyshell M.L. Ryan M.P. Ingham, B. In situ synchrotron X-ray diffraction experiments on electrochemically deposited ZnO nanostructures. *Journal of Physical Chemistry C*, 112(38):14863–14866, 2008.

[18] Jin-Hong Lee, Kyung-Hee Ko, and Byung-Ok Park. Electrical and optical properties of ZnO transparent conducting films by the sol-gel method. *Journal of Crystal Growth*, 247(1-2):119 – 125, 2003.

[19] Agarwal Lily Bhattacharyya A.B. Srivastava, J.K. Electrical characteristics of lithium-doped ZnO films. *Journal of the Electrochemical Society*, 136(11):3414–3417, 1989.

[20] Tadatsugu Minami, Hidehito Nanto, and Shinzo Takata. Highly Conductive and Transparent Aluminum Doped Zinc Oxide Thin Films Prepared by RF Magnetron Sputtering. *Japanese Journal of Applied Physics*, 23(Part 2, No. 1):L280–L282, 1984.

[21] Garcia F.J. Tomar, M.S. A ZnOCuSe2 thin film solar cell prepared entirely by spray pyrolysis. *Thin Solid Films*, 90(4):419–423, 1982.

[22] L. Olvera, A. Maldonado, R. Asomoza, M. Konagai, and M. Asomoza. Growth of textured ZnO:In thin films by chemical spray deposition. *Thin Solid Films*, 229(2):196 – 200, 1993.

[23] A. E. Jimenez-Gonzalez, Jose A. Soto Urueta, and R. Suarez-Parra. Optical and electrical characteristics of aluminum-doped ZnO thin films prepared by solgel technique. *Journal of Crystal Growth*, 192(3-4):430 – 438, 1998.

[24] Segawa Y. Yoshida S. Tsukazaki A. Ohtomo A. Kawasaki M. Makino, T. Gallium concentration dependence of room-temperature near-band-edge luminescence in n-type ZnO:Ga. *Applied Physics Letters*, 85(5):759–761, 2004.

[25] J. Owen, M. S. Son, K.-H. Yoo, B. D. Ahn, and S. Y. Lee. Organic photovoltaic devices with Ga-doped ZnO electrode. *Applied Physics Letters*, 90(3):033512, 2007.

[26] Ilican S. Caglar Y. Caglar, M. Influence of dopant concentration on the optical properties of ZnO: In films by sol-gel method. *Thin Solid Films*, 517(17):5023–5028, 2009.

[27] Lira-Cantu M. Gonzalez-Valls, I. Vertically-aligned nanostructures of ZnO for excitonic solar cells: A review. *Energy and Environmental Science*, 2(1):19–34, 2009.

[28] L. Goris, R. Noriega, M. Donovan, J. Jokisaari, G. Kusinski, and A. Salleo. Intrinsic and Doped Zinc Oxide Nanowires for Transparent Electrode Fabrication via Low-Temperature Solution Synthesis. *Journal of Electronic Materials*, 38:586–595, 2009.

[29] Ma J.A Ji F.A Wang Y.A Cheng C.B Ma H.A Yu, X.A. Thickness dependence of properties of ZnO:Ga films deposited by rf magnetron sputtering. *Applied Surface Science*, 245(1-4):310–315, 2005.

[30] Niki S Oh J.-Y. Song J.-O. Seong T.-Y. Park S.-J. Fujita-S. Kim S.-W. Kim, K. High electron concentration and mobility in Al-doped ZnO epilayer achieved via dopant activation using rapid-thermal annealing. *Journal of Applied Physics*, 97(6):1–3, 2005.

[31] Olvera M.D.L.L. Maldonado-A. Asomoza R.-Acosta D.R. Guillen-Santiago, A. Electrical, structural and morphological properties of chemically sprayed F-doped ZnO films: Effect of the ageing-time of the starting solution, solvent and substrate temperature. *Physica Status Solidi (A) Applied Research*, 201(5):952–959, 2004.

[32] Ning Z.Y. Jiang M.F. Fan, D.H. Characteristics and luminescence of Ge doped ZnO films prepared by alternate radio frequency magnetron sputtering. *Applied Surface Science*, 245(1-4):414–419, 2005.

[33] Chao Wang, Zhenguo Ji, Kun Liu, Yin Xiang, and Zhizhen Ye. p-Type ZnO thin films prepared by oxidation of Zn3N2 thin films deposited by DC magnetron sputtering. *Journal of Crystal Growth*, 259(3):279 – 281, 2003.

[34] Yoshitaka Nakano, Takeshi Morikawa, Takeshi Ohwaki, and Yasunori Taga. Electrical characterization of p-type N-doped ZnO films prepared by thermal oxidation of sputtered Zn3N2 films. *Applied Physics Letters*, 88(17):172103, 2006.

[35] K.G. Saw, K. Ibrahim, Y.T. Lim, and M.K. Chai. Self-compensation in ZnO thin films: An insight from X-ray photoelectron spectroscopy, Raman spectroscopy and time-of-flight secondary ion mass spectroscopy analyses. *Thin Solid Films*, 515(5):2879 – 2884, 2007.

[36] Yan X.D. Han J.-Chen R.Q. Gao-W. Metson J. Zou, C.W. Study Of A Nitrogen-doped ZnO Film With Synchrotron Radiation. *Applied Physics Letters*, 94(17), 2009.

[37] Xu H. Chin W.S.-Yong Z. Wee-A.T.S. Liu, T. Local structural evolution of Co-doped ZnO nanoparticles upon calcination studied by in situ quick-scan XAFSg. *Journal of Physical Chemistry C*, 112(10):3489–3495, 2008.

[38] Hlne Serier, Manuel Gaudon, and Michel Mntrier. Al-doped ZnO powdered materials: Al solubility limit and IR absorption properties. *Solid State Sciences*, 11(7):1192 – 1197, 2009.

[39] Frank Maldonado and Arvids Stashans. Al-doped ZnO: Electronic, electrical and structural properties. *Journal of Physics and Chemistry of Solids*, 71(5):784 – 787, 2010.

[40] M. Kao, H. Chen, and S. Young. Effects of preannealing temperature of ZnO thin films ontheperformance of dye-sensitized solar cells. *Applied Physics A: Materials Science & Processing*, 98:595–599, 2010.

[41] H. Cheng, X.J. Xu, H.H. Hng, and J. Ma. Characterization of Al-doped ZnO thermoelectric materials prepared by RF plasma powder processing and hot press sintering. *Ceramics International*, 35(8):3067 – 3072, 2009.

[42] Aslan M.H. Ozer M.-Ora A.Y. Bahsi, Z.B. Sintering behavior of ZnO: Al ceramics fabricated by sol-gel derived nanocrystalline powders. *Crystal Research and Technology*, 44(9):961–966, 2009.

[43] Jeremy K. Burdett, Geoffrey D. Price, and Sarah L. Price. Role of the crystal-field theory in determining the structures of spinels. *Journal of the American Chemical Society*, 104(1):92–95, 1982.

[44] Jin-Hong Lee and Byung-Ok Park. Transparent conducting ZnO:Al, In and Sn thin films deposited by the sol-gel method. *Thin Solid Films*, 426(1-2):94 – 99, 2003.

[45] Sawada Y. Nishide T. Seki, S. Indium-tin-oxide thin films prepared by dip-coating of indium diacetate monohydroxide and tin dichloride. *Thin Solid Films*, 388(1-2):22–26, 2001.

[46] Keh moh Lin and Paijay Tsai. Growth mechanism and characterization of ZnO: Al multi-layered thin films by sol-gel technique. *Thin Solid Films*, 515(24):8601 – 8604, 2007.

[47] Fleischer K. Fleischer K.-Shvets I.V. Arca, E. Influence of the precursors and chemical composition of the solution on the properties of ZnO thin films grown by spray pyrolysis. *Journal of Physical Chemistry C*, 113(50):21074–21081, 2009.

[48] Hongxia Li, Jiyang Wang, Hong Liu, Changhong Yang, Hongyan Xu, Xia Li, and Hongmei Cui. Sol-gel preparation of transparent zinc oxide films with highly preferential crystal orientation. *Vacuum*, 77(1):57 – 62, 2004.

[49] Park B.-O. Lee, S.-Y. Electrical and optical properties of In2O3-ZnO thin films prepared by sol-gel method. *Thin Solid Films*, 484(1-2):184–187, 2005.

[50] Koh L.H.K. Crean-G.M. O'Brien, S. ZnO thin films prepared by a single step sol-gel process. *Thin Solid Films*, 516(7):1391–1395, 2008.

[51] Chien-Yie Tsay, Kai-Shiung Fan, Sih-Han Chen, and Chia-Hao Tsai. Preparation and characterization of ZnO transparent semiconductor thin films by sol-gel method. *Journal of Alloys and Compounds*, 495(1):126 – 130, 2010.

[52] Hua Wang, Muhui Xu, Jiwen Xu, Ling Yang, and Shangju Zhou. Effects of annealing temperature and thickness on microstructure and properties of solgel derived multilayer Al-doped ZnO films. *Journal of Materials Science: Materials in Electronics*, 21:145–148, 2010.

[53] Hua Wang, Mu-hui Xu, Ji-wen Xu, Ming-fang Ren, and Ling Yang. Low temperature synthesis of solgel derived Al-doped ZnO thin films with rapid thermal annealing process. *Journal of Materials Science: Materials in Electronics*, 21:589–594, 2010.

[54] M. H. Mamat, M. Z. Sahdan, Z. Khusaimi, and M. Rusop. Electrical characteristics of sol-gel derived aluminum doped zinc oxide thin films at different annealing temperatures. *Electronic Devices, Systems and Applications (ICEDSA), 2010 Intl Conf on*, pages 408 –411, apr. 2010.

[55] Cameron D.C. Tang, W. Aluminum-doped zinc oxide transparent conductors deposited by the sol-gel process. *Thin Solid Films*, 238(1):83–87, 1994.

[56] A. E. Jimnez-Gonzlez. Modification of ZnO Thin Films by Ni, Cu, and Cd Doping. *Journal of Solid State Chemistry*, 128(2):176 – 180, 1997.

[57] Z Ben Ayadi, L El Mir, K Djessas, and S Alaya. Electrical and optical properties of aluminum-doped zinc oxide sputtered from an aerogel nanopowder target. *Nanotechnology*, 18(44):445702, 2007.

[58] Kozuka-H. Yoko-T. Ohyama, M. Sol-gel preparation of transparent and conductive aluminum-doped zinc oxide films with highly preferential crystal orientation. *Journal of the American Ceramic Society*, 81(6):1622–1632, 1998.

[59] C. Periasamy and P. Chakrabarti. Tailoring the Structural and Optoelectronic Properties of Al-Doped Nanocrystalline ZnO Thin Films. *Journal of Electronic Materials*, pages 1–8, 2010.

[60] B. Szyszka. Transparent and conductive aluminum doped zinc oxide films prepared by mid-frequency reactive magnetron sputtering. *Thin Solid Films*, 351(1-2):164–169, 1999.

[61] Yulong Zhang, Ye Yang, Junhua Zhao, Ruiqin Tan, Weiyan Wang, Ping Cui, and Weijie Song. Optical and electrical properties of aluminum-doped zinc oxide nanoparticles. *Journal of Materials Science*, pages 1–7, 2010.

[62] Tuller-H.L. Sukkar, M.H. Defect equilibria in ZnO varistor materials. volume 7, pages 71–90, 1983.

[63] Banerjee-A. Chopra-K.L. Major, S. Optical and electronic properties of zinc oxide films prepared by spray pyrolysis. *Thin Solid Films*, 125(1-2):179–185, 1985.

[64] B. Rech and H. Wagner. Potential of amorphous silicon for solar cells. *Applied Physics A: Materials Science & Processing*, 69:155–167, 1999.

[65] K. Ramanathan, F. S. Hasoon, S. Smith, D. L. Young, M. A. Contreras, P. K. Johnson, A. O. Pudov, and J. R. Sites. Surface treatment of CuInGaSe2 thin films and its effect on the photovoltaic properties of solar cells. *Journal of Physics and Chemistry of Solids*, 64(9-10):1495 – 1498, 2003.

[66] Klaer-J. Scheer-R.-Lux-Steiner M.C.-Luck I. Meyer-N. Rhle U. Klenk, R. Solar cells based on CuInS2 an overview. *Thin Solid Films*, 480-481:509–514, 2005.

[67] Sharon E. Ashbrook. Recent advances in solid-state NMR spectroscopy of quadrupolar nuclei. *Phys. Chem. Chem. Phys.*, 11:6892–6905, 2009.

[68] K.J.D. MacKenzie and M.E. Smith. *Multinuclear solid-state NMR of inorganic materials*. Pergamon materials series. Pergamon, 2002.

[69] Ohtaki-M. Eguchi-K.-Arai-H. Tsubota, T. Thermoelectric properties of Al-doped ZnO as a promising oxide material for high-temperature thermoelectric conversion. *Journal of Materials Chemistry*, 7(1):85–90, 1997.

[70] Jonathan F. Stebbins. Aluminum Substitution in Rutile Titanium Dioxide: New Constraints from High-Resolution 27Al NMR. *Chemistry of Materials*, 19(7):1862–1869, 2007.

[71] E.H. Hall. On a New Action of the Magnet on Electric Currents. *American Journal of Mathematics*, 2:287–292, 1879.

[72] L.J. Van der Pauw. A method of measuring specific resistivity and Hall effect of discs of arbitrary shape. *Philips Research Reports*, 13:1–9, 1958.

[73] Al-Salim N.I. Kemmitt, T. Production of photocatalyst, 2000.

[74] M.P. Pechini. Method of preparing lead and alkaline earth titanates and coating method using the same to form a capacitor, 1967.

[75] Mills-A.M. Gainsford-G.J. Kemmitt, T. The formation of manganese carboxylates from MnO and MnO2 and their application in lithium manganate precursors: X-ray crystal structure of manganese lactate trihydrate. *Australian Journal of Chemistry*, 54(1):37–42, 2001.

[76] M. Rajendran and M. Subba Rao. Formation of BaTiO3 from Citrate Precursor. *Journal of Solid State Chemistry*, 113(2):239 – 247, 1994.

[77] Yuming Sun and Hezhou Wang. The electronic properties of native interstitials in ZnO. *Physica B: Condensed Matter*, 325:157 – 163, 2003.

[78] Tapan K. Gupta. Application of Zinc Oxide Varistors. *Journal of the American Ceramic Society*, 73(7):1551–2916, 1990.

[79] JianLin Chen, Ding Chen, and ZhenHua Chen. Optimization of the process for preparing Al-doped ZnO thin films by sol-gel method. *Science in China Series E: Technological Sciences*, 52:88–94, 2009.

[80] Lawrence B. Alemany and Garry W. Kirker. First observation of 5-coordinate aluminum by MAS aluminum-27 NMR in well-characterized solids. *Journal of the American Chemical Society*, 108(20):6158–6162, 1986.

[81] G. Urretavizcaya, A. L. Cavalieri, J. M. Porto Lpez, I. Sobrados, and J. Sanz. Thermal Evolution of Alumina Prepared by the Sol-Gel Technique. *Journal of Materials Synthesis and Processing*, 6:1–7, 1998.

[82] Feitknecht L. Schlchter-R.-Kroll-U. Vallat-Sauvain E. Shah-A. Fa, S. Rough ZnO layers by LP-CVD process and their effect in improving performances of amorphous and microcrystalline silicon solar cells. *Solar Energy Materials and Solar Cells*, 90(18-19):2960–2967, 2006.

[83] Linklater R. Kemmitt, T. Conference on Nanoscience and Nanotechnology (ICONN). *IEEE Xplore*, In Press.

[84] Park B.N. Yoo-D.-G.-Boo J.-H. Jung D. Jeong, S.H. Al-ZnO thin films as transparent conductive oxides: Synthesis, characterization, and application tests. *Journal of the Korean Physical Society*, 50(3):622–625, 2007.

[85] Ashley C.S. Brinker-C.J. Logan, D.L. Sol-gel films with tailored microstructures. *Mater. Res. Soc. Symp. Proc.*, 271:541–546, 1992.

[86] Raoufi T Raoufi, D. The effect of heat treatment on the physical properties of sol-gel derived ZnO thin films. *Applied Surface Science*, 255(11):5812–5817, 2009.

[87] Kim D.-E. Lin, L.-Y. Effect of annealing temperature on the tribological behavior of ZnO films prepared by sol-gel method. *Thin Solid Films*, 517(5):1690–1700, 2009.

[88] Miao L. Tanemura-S.-Tanemura-M. Cao-Y. Tanaka S. Shibata N. Ran, F. Effect of annealing temperature on optical properties of Er-doped ZnO films prepared by sol-gel method. *Materials Science and Engineering B: Solid-State Materials for Advanced Technology*, 148(1-3):35–39, 2008.

[89] A Van der Drift. Evolutionary selection, a principle governing growth orientation in vapour-deposited layers. *Philips Res. Rep.*, 22:267, 1967.

[90] Orlinov V. Misiuk-A. Petrov, I. Highly oriented ZnO films obtained by D.C. reactive sputtering of a zinc target. *Thin Solid Films*, 120(1):55–67, 1984.

[91] Islam, S. Ishizuka, A. Yamada, K. Matsubara, S. Niki, T. Sakurai, and K. Akimoto. Thickness study of Al:ZnO film for application as a window

layer in Cu(In1-xGax)Se2 thin film solar cell. *Applied Surface Science*, 257(9):4026 – 4030, 2011.

[92] Aihua Zhong, Jin Tan, Huali Huang, Shengchang Chen, Man Wang, and Sai Xu. Thickness effect on the evolution of morphology and optical properties of ZnO films. *Applied Surface Science*, 257(9):4051 – 4055, 2011.

[93] Xiao Q. Zhou-H.-Wang-D. Jiang-W. Huang, S. Hydrothermal synthesis and conductive properties of Al-doped ZnO rod-like whiskers. *Journal of Alloys and Compounds*, 486(1-2):L24–L26, 2009.